ABSTRACT

Factor Influencing Headcut Migration within a Cohesive
Texas Black-Land Gully

Lance Auguste, M.S.

Mentor: Peter Allen, Ph.D.

Gully erosion degrades the Black-Land Prairies (BLP) (Texas), affecting agricultural productivity. It is initiated by rill and inter-rill erosive processes and exacerbated by storm frequency and duration. Few studies have assessed the factors influencing headcut development in cohesive gullies, mainly due to the limitations posed by field instrumentation and the high shear strength of clay soils. Cohesive gullies, e.g. those found in Vertisols may be regarded as an end member gully types in erosion studies. As such, critical assessments of the evolution and failure mechanisms of these headcuts are necessary for channel evolution modeling and determining the potential contribution of these channels to sediment budgets. The El Niño season provided ideal atmospheric perturbations to foster such a study. For the first time, this paper attempts to demonstrate relationships between aerial and subaerial factors influencing gully growth, using new remote sensing methods, hydrology, and in-situ soil properties.

As such, the objective is to elucidate the environmental influences leading to erosion in a permanent cohesive gully, by systematically investigating the headcut through space-time and time-lapse observations. Geomorphological processes were validated through offsite observations. Precipitation, migration, discharge and volumetric soil moisture was measured to investigate relationships impacting retreat. Drying days was found to be the most critical factor, with an R^2 of 0.95. The total rainfall between migration periods, and discharge at the over-fall also critically informed migration, with R^2 values of 0.89, and 0.78, respectively. A vertical zonation of the headcut was found based on soil geotechnical properties that produced a distinct failure mechanism. Tridimensional photo reconstruction (3D PR) (Structure-From-Motion) techniques were used for topographic analysis.

Factors Influencing Headcut Migration within a Cohesive Texas Blackland Gully

by

Lance Auguste, B.S.

A Thesis

Approved by the Department of Geosciences

_____

Stacy Atchley, Ph.D., Chairperson

Submitted to the Graduate Faculty of
Baylor University in Partial Fulfillment of the
Requirements for the Degree
of

Master of Science

Approved by the Thesis Committee

_____

Peter Allen, Ph.D., Chairperson

_____

Joseph White, Ph.D.

_____

Scott James, Ph.D.

Accepted by the Graduate School

December 2017

_____

J. Larry Lyon, Ph.D., Dean

Page bearing signatures is kept on file in the Graduate School.

TABLE OF CONTENTS

LIST OF FIGURES

LIST OF TABLES

ACKNOWLEDGMENTS

In the words of Sir Derek Walcott, a renowned Saint Lucian scholar: “The strength of the scientific establishment in any country is related to its general level of education, not only in supplying large numbers of eager minds for further training, but also in ensuring a public opinion that holds science in esteem and approves financial support.” It is in this regard that I thank Baylor University and its patrons for fostering an environment conducive to intellectual growth, and extending an arm in my pursuit of science.

Of notable mention are the members of my scientific caucus (committee): Dr Peter Allen, Dr Joseph White and Dr Scott James. I thank you for providing me with the tools and attention to take this next step in my academic endeavors. Your involvement in my study, and commitment to scientific discipline is exemplary. To all those too numerous to mention, which I have had the privilege of engaging in conversation (science or otherwise) such as Jeffrey Arnold (Ph.D), Joe Yelderman (Ph.D), John Dunbar (Ph.D), Jonathan Cook (Ph.D), Bruce Byers, Paulette Penney (the linchpin of the department) and my distinguished student colleagues; I express thanks.

To the members of the Engineering-Hydrology class of Fall 2015 and others who assisted with field preparation, I extend my appreciation for the assistance in navigating Brookeen Creek. Thank you for enduring the weather and often muddy channels.

DEDICATION

To my parents (Joseph and Marcella Auguste), thank you for your unyielding support through this degree. Your wisdom, guidance and attentiveness was a refuge during the trials of this mountain. Your encouragement was sincerely appreciated.

Most endearingly, to the matriarch of my Saint Lucian family (Fredericka Leonce), thank you for the support and conversation.

CHAPTER ONE

Factors Influencing Headcut Migration within a Cohesive Texas Black-Land Gully

1.0 Introduction

Sediment is one of the largest pollutants of streams and rivers. An estimated 44 and 45 billion is spent on erosion remediation in the United States and the European Union, respectively (Telles et al., 2011). Gully erosion represents an increasing contribution to net sediment loss, supplying 19-81 percent of sediment yield in North America (Poesen et al., 1996). In the State of Texas, gully and stream bank erosion contribute about 98 million tons of sediment per anum (Greiner, 1982). As such, erosion due to the formation of gullies may represent an increasing contribution to net sediment loss. Sediment output from these systems has been shown to be a vital component in sediment budget analyses (Verstraeten et al., 2003) and stream ecological assessments (Castro and Reckendorf, 1995).

Gully erosion is a concentrated flow phenomenon, impacted by land use and antecedent conditions (Saxton et al., 2012; Nyssen et al., 2006). It has been shown to be an impediment to agricultural sustainability and growth. Soil loss due to gullying decreases crop yields, the potential for farm consolidation, and the availability of productive lands (Zgłobicki et al., 2014; Valentin et al., 2005). After they have developed, remediation methods typically reduce soil quality (Ollobarren et al., 2016; Xu et al., 2016) and lead to soil coarsening when the process is continuous. According to Castillo & Gómez (2016), the rates of soil loss due to permanent gully erosion exceed the rates typical of agricultural drainage basins. The Texas Black-Land Prairie, although an agriculturally productive region, remains unrepresented in gully studies.

Several classification schemes have been used to define gullies. Gullies are channels with near vertical scarps, where water flowing over the brink of the headcut instigates progressive headward migration of the scarp. They are distinguished temporally (permanent: ephemeral) and spatially (valley bottom: hillslope) (Poesen et al., 2003; Brice, 1966; Wu & Cheng, 2005). However, they represent a continuum from the hillslope to the valley-bottom variety. The impact of streams on the stability of valley-bottom gullies through degradation, profile-width changes, stream merging, and bifurcation distinguishes valley-bottom from hill-slope gullies. Gullies can be further categorized by texture (cohesive: non-cohesive), which is important because the retreat rate of headcuts depend on the strength of the material incised (Radoane et al., 1995). Cohesive soils are fine-grained soils with high shear strengths and chemical bonding in moist and dry conditions, e.g., clays and silts. These soils behave plasticly when wet and are hard when dry (OSHA, 2017). Cohesionless soils show little binding ability, e.g., sand, gravel. Herein, cohesive gullies refer to those with cohesive characteristics, e.g., dark clay soils (Vertisols) (Dudual, 1963). Vertisols cover 3.35 million km^2 globally (IUSS, 2014) and are the most common soil order within the Black-Land Prairies where in excess of 48,000 km^2 exist. Few studies have investigated lithology as a factor influencing the evolution of headcuts (Castillo and Gómez, 2016).

While many of the world's gullies occur predominantly in loess environments and have been documented mainly in temperate regions (Castillo and Gómez, 2016; Vanwalleghem et al., 2005), studies in cohesive gullies are sparse. Cohesive gullies occur in many tropical and semiarid regions (El-Swaify et al., 1982; IBSRAM 1987). Studies predominate in Nigeria (Nyssen et al., 2006; Frankl et al., 2012), Ethiopia (Zegeye et al.,

2016; Frankl et al., 2013), China (Dong et al., 2014; Ding et al., 2017) and Australia (Whitford et al., 2010; Hughes et al., 2009). Other areas include Mexico (Geissen et al., 2007) and California (Perroy et al., 2010). Because these soils are susceptible to severe erosion and are frequently used in agriculture, management is necessary. As such, an understanding of the factors impacting the development and migration of these gully types is necessary.

An increasing number of investigations have assessed topography as an initiation mechanism in gully studies, particularly the drainage area-slope relationship (Castillo and Gómez, 2016). Two major hypotheses have been proposed, which are largely functions of flow shear stress relationships and topographic thresholds. For gullies to develop, the average overland and subsurface flow stress should be greater than the resistive forces for sediment entrainment (Poesen et al., 2002). Drainage area-slope (Da-S) thresholds were developed to predict gully initiation for different regions (McNamara et al., 2006; Patton and Schümm, 1975; Wu and Cheng, 2005). The Da-S threshold supposes that larger basins exert greater flow shear stresses, therefore allowing gully development on smaller catchment slopes. Less attention has been paid to subaerial processes.

The migration of a headcut may vary spatially and temporally under varying climatic and subaerial conditions. According to Vanmaercke et al., (2016), the processes involved in the retreat of gully scarps are complex. However, they may be divided into processes that cause and control migration. Headcut retreat may be influenced by soil cracking, plunge pool erosion, soil piping, splash erosion, fluting, and mass failures (Vanmaercke et al., 2016). Controlling factors included erosive and resistive forces. Erosive forces reflect factors that impact flow rates, e.g., the contributing catchment,

weather, antecedent soil moisture, land cover, soil characteristics, and slope (Vanmaercke et al., 2016). However, resistive forces at the gully head are mainly due to vegetation, soil properties, and rock cover (Vanmaercke et al., 2016).

The properties of cohesive soils further complicate migration within these systems. Soil erodibility is affected by the in-situ physical, geochemical , engineering and biologic conditions of soil (Grabowski et al., 2011), e.g., grain size, bulk density, water content, temperature, cohesion. Changes in soil moisture affect the structure and shrink-swell potential of clays (Rosone et al., 2016). Increasing moisture decreases soil suction and shear strength while decreasing moisture leads to fissuring. Further, increases in the temperature of eroding water increase erodibility (Grissinger, 1966). Within the Black-Land Prairies, soil cracking has been shown to influence runoff predictions (Arnold et al., 2005a), providing conduits for bypass flow, rainfall interception, and infiltration as soils expand and contract (Dinka et al., 2013). Further, high antecedent moisture states have been associated with greater crack densities (Kishné et al., 2010).

After a gully develops in cohesive sediment, and during migration, headcut failure progresses in various ways. The growth of rills and side slope slumping has been postulated (Pathak et al., 2005). Scour hole expansion, and plunge pool erosion have been identified as mechanisms by which instability is induced at gully heads. This has been related to increases in height (Ploumis-Devick, 1985). Crack formation and surface-seal failure were considered to be important parts of the retreat mechanism within stepped headcuts (Bennett et al. 2000). Subsurface erosion by soil piping was demonstrated as a method promoting gully development and expansion (Swanson et al., 1989; Frankl et al., 2012). Increasing piezometric stresses due to groundwater table fluctuations further contribute to

headcut failure by reducing shear strength (Zegeye et al., 2016; Tebebu et al., 2010). Additionally, the strength of cohesive soils pose various field scale limitations, such as installing instrumentation. Moreover, intra-annual atmospheric changes and land management practices seasonally influence soil properties, acting as a heterogeneous flux to the system. As such, studies documenting the progressive evolution of headcuts are conducted in flumes, while those documenting migration are typically done using remote sensing and topographical methods.

The gully head is the point of initiation, retreat, and network connectivity within a gully system. During hydraulically driven erosion cycles, headcuts form when erosion thresholds are exceeded. Migration occurs due to the causative agents of erosion. As the gully head expands within catchments, linkages between hillslopes and channels develop (Poesen et al., 2002). Consequently, soil loss and sedimentation of streams occur. Given the importance of the headcut as a distinct zone within a gully, it was the focus of this investigation.

Rainfall was considered paramount in predicting headcut evolution and migration. Apart from driving the erosion process, rainfall further impacts the subaerial condition of the soil through its effect on moisture (Rengers & Tucker, 2015). Relationships between soil moisture, runoff, infiltration, and soil engineering properties were concurrently explored with high-level field and time-lapse monitoring techniques. Structure-from-motion, a photogrammetric method enabling the scaled reconstruction of three-dimensional scenes from two-dimensional images (Ullman, 1979) was used for capturing transient morphologic changes of the headcut.

The objectives of this study are to:

1. Describe the environmental, hydrologic, and evolutionary relationships impacting migration within a cohesive Texas Black-Land Prairie gully. The relationships between soil moisture, infiltration, precipitation, discharge and headcut migration are explored.
2. Present a conceptual model for the development and migration of these gullies using structure-from-motion and space-time analyses. The role of lithology is explored as a parameter influencing the space-time evolution of gully headcuts during migration.

1.1. *Study Area*

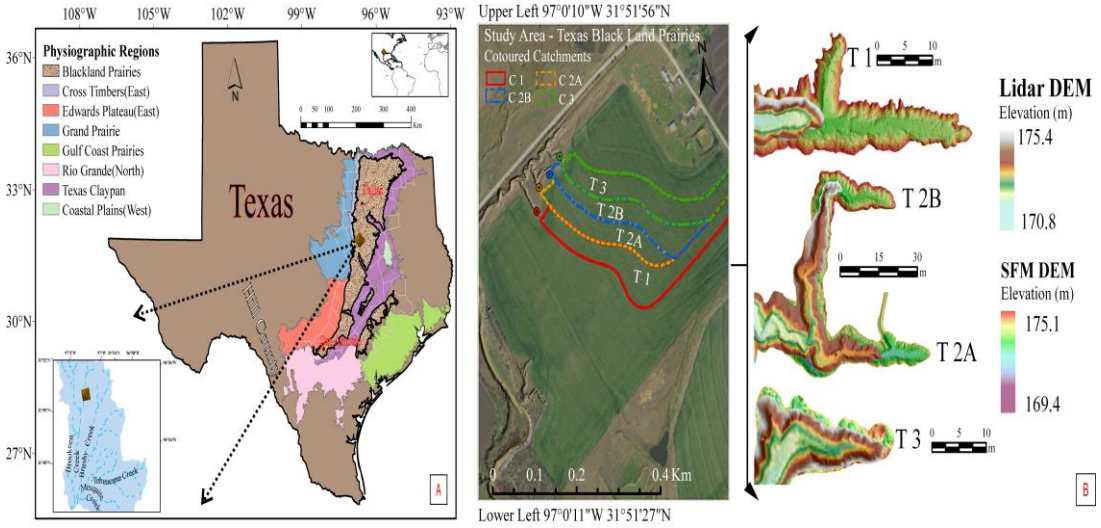

Figure 1: Study area depicting: (A) the regional location and B) Digital elevation models of Structure-from -motion and Lidar (TRNIS) overlay for the tributaries investigated (T1-T3) and correspondent catchments (C1-C3).

The gullies investigated are situated in North Central Texas, Hill County. Central Texas is made up of the Black-Land Prairies, Eastern Cross Timbers, and Grand Prairie physiographic regions. The surrounding physiography influences the topography of the Black-Land Prairies (Montgomery, 1993). Few studies have been conducted within this region. However, it may represent a unique geomorphic zone. The Black-Land Prairies are

divided into northern and southern prairies. The northern prairie extends from Bexar County in the south to Lamar County in the North and is about 565 km long and 152 km wide at its greatest breadth. Figure 1A depicts the study area and the adjacent physiographic regions. A 1^{st} -2^{nd} order gully network along a 7.9 km reach within the Brookeen-Tehuacana Creek sub-catchment (105 km^2) was investigated. The average slope of the reach was 3%.

Three gully tributaries labeled as T1 to T3 in Figure 1B were investigated. The tributaries each joined a 360-m gully emanating from Brookeen Creek. Tributary 1 was the primary tributary under investigation. Tributaries 2 and 3 were monitored intermittently for comparison. The drainage areas depicted as C1-C3 in Figure 1B are delineated along terraces. Over a period of 3.6 years, the gully tributaries have degraded a maximum of 1.4 m at the mouth of channels.

1.1.1 Climate

The climate of the Black-Land Prairies may be described as humid-subtropical to continental. Rainfall is associated with the movement of Canadian and Pacific maritime fronts; convective storms may further contribute to rainfall totals during summer storm periods. Rainfall is concentrated in Spring and Fall, while summer months are driest. Average annual precipitation varies from 500 mm in the south to 1015 mm in the north (J. C. J. Yelderman, 1993). Evapotranspiration may exceed 1500 mm on an annual basis during the dry summers.

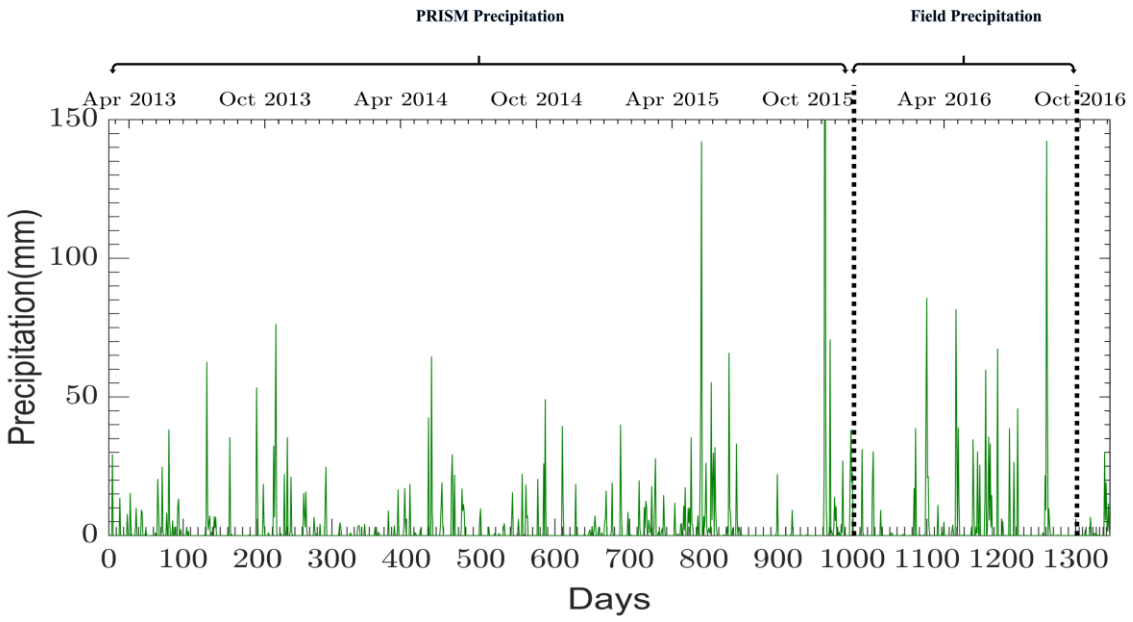

Figure 2: Precipitation pattern for the period of interest: From Lidar flight through the observation period (Drone fight)

The investigated area is located in North Central, Texas. Mean annual precipitation and temperature are 950 millimeters and 18 ºC, respectively. Precipitation peaks in March and October (~ 110 mm), with lows in July (~ 40mm) (PRISM Climate Group, 2017). Temperature peaks from July to August (about 29 ºC). Figure 2 depicts the period of interest. Rainfall totaled 4,500 mm, with a daily average of about 3 mm. The figure distinguishes precipitation totals obtained from Prism Climate Group and field monitoring. A cyclic precipitation pattern was evident for the first 1,127 days, with an increase in rainfall frequency around day 800 and a dry period starting around day 850. During the field monitoring period (February-September), precipitation intensity, duration, and frequency increased. 1,130 millimeters of rain was recorded. Ambient air temperature varied from 3 to 40º C.

1.1.2 Geology

Within the Black-Land Prairies (Figure 1A), surface elevation varies from 76 to 245 meters. The Eagle Ford, Austin, Taylor, Navarro and Midway geologic groups are the primary geological units (Hill and Walcott, 1901). Bedrock within the study area (Figure 1B) is mapped as the Black-Land Taylor marl (University of Texas, 1979), a marine calcareous shale with minor quartz and pyrite clastics perceived to emanate from the southern Rocky Mountains (McFarland, 1993). The Taylor Marl dips to the southeast at rates ranging from 8-15 m km^{-1}. Four dominant zones are associated with these shale bedrock in North Central Texas: a soil layer, weathered zone, transition zone, and un-weathered zone (Allen et al., 2005).

1.1.3 Soils

The regional geology of the Black-Land Prairie exerts a strong influence on soil characteristics. Most soils developed from shales rich in carbonates and clays (Hallmark, 1993). Vertisols are the most common soil order and developed on the Eagle Ford and Tylor formations. The Houston Black-Heiden-Ferris soil series is the most common soil association (Collins et al., 1975).

Normangee clay loams and Houston black clays (smectic, thermic, udertic, haplustalfs) were the primary soil series identified in the study area (Figure 1B) (NRCS, 2017). These soils have gilgai, and slickenside morphologies, a blocky structure and are moderately well drained. Cracks extended vertically through the gully head-scarp when dry. Eroded sediment was orange-yellow and gray, exposing indurated Taylor Marl at points along the channel and Brookeen creek.

1.1.4 Soil Horizons: Engineering and Physical Properties

The United States Department of Agriculture mapped soil horizons and geotechnical properties (NRCS, 2017) are listed in Table 1. Soil horizons are based on USDA delineated map units (Normangee Clays), which are named according to soil taxonomy classes of dominant soils. Engineering properties refer specifically to the liquid and plastic limits. The engineering properties follow the hydrologic soil group classification, in this case Group-D within the National Engineering Manual (USDA-NRCS, 2009), which is based on component soil properties. Here, soil physical properties refer to soil texture and bulk density. Erodibility is estimated in Table 1 using the Universal Soil Loss Equation (USLE) and Revised Universal Soil Loss Equation (RUSLE), which are indicators of the vulnerability of soil to rill and inter-rill erosion. Generally, the engineering and physical soil properties are estimates derived from field test data at the site or within nearby locations. These properties vary with depth within the soil profile.

Table 1: Engineering and physical soil properties of USDA Mapped Soil horizons for the study area. LL is the liquid limit, PI is the Plasticity Index

Horizons	Depth (m)	LL	PI	% Sand	% Silt	% Clay	Bulk Density (g cm^{-2})	Erodibility
Ap	0.18	40-41	21-22	20-34	25-27	28-29	1.38-1.40	0.37
Bt	1.30	50-62	29-39	20-25	17-28	35-47	1.39-1.44	0.28
Cdk	>1.3	50-64	34-41	15-23	10-28	42-49	1.63	0.32

Soils show an Ap, Bt, and Cdk soil series stratified at 0.18, 1.3, and >1.3 m from the surface. The depth to the restrictive layer was mapped at 1-1.7 m (NRCS, 2017). The liquid limit, plastic limit, and bulk density generally increased below the soil surface. Soil Atterberg limits relate to the behavior and strength of cohesive soils. The plastic limit is the moisture condition where soil behaves plasticly, representing the brittleness of soil

(Haigh et al., 2013). However, the liquid limit represents the moisture condition where soil behaves liquid, indicating soil strength (Haigh, 2012). Below these limits, soil is theoretically solid. Table 1 shows that sand content also decreased while percent clay increased with depth. The maximum silt content was similar at each horizon, although lower boundaries occurred within the Cdk horizon. For most soil properties except bulk density and the estimated erodibilities, the upper limits of the Bt-Cdk horizon were undifferentiable. Soil erodibility decreased and increased within the profile.

Based on process-based observations and measurements of engineering and physical field properties, the soil horizons at the study area have been refined. Three soil zones depicted in Figure 3 correlate with USDA engineering, physical, and map unit properties. Similar to Table 1, soil properties show the same general trends. Generally, a decrease in scarp weathering from the headcut top to the base was associated with increasing Atterberg limits, clay content, bulk density, and moisture. However, a distinctive B horizon was not observed. As such, the soil horizon is largely an AC sequence, a finding common for Vertisol cantenas (Dudual, 1963). The soil zones can be delimited based on soil activity (Skempton, 1953), which is the ratio of the plasticity index and percent clay. Soil activity was 1.9, 2.4, 1.9 and 1.6 in succession from zones I to IV. According to Allen et al.,(1999), activities higher than 1.25 have lower shear resistances, higher water retention, and lower permeability; the liquid limit was found to be a critical soil state related to erodibility.

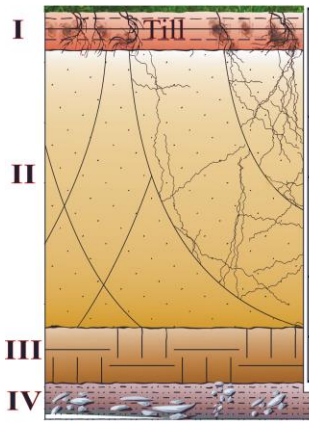

Zones	USDA Horizons	Soil Descriptors	Atterberg Limits			Texture (%)			Bulk Density	Moisture
			LL	PL	PI	Clay	Silt	Sand		
I	A	Cultivated, Disturbed, Crop root depth	53	25	28	24	59	17	1.3	Low
II		Shrinkage cracks, blocky-prismatic structure, slickensides, parallelepiped, rapid drying	70	27	43	31	64	5	1.4	Medium
III	C	Moist lower zone, Transition to Taylor Marl	73	30	43	37	60	3	1.5	High
IV	D	Weathered Taylor Marl	77	31	46	49	50	1	---	----

Figure 3: Soil hydrogeomorphic zones based on the observed correlation between USDA soil horizons and measured soil characteristics for tributary 1 (Figure 1). Four zones were identified each considered lithologically distinct and having varying responses during erosion. Two distinctive layers are apparent. Zones 2 and 3 transition into each other. Zones 4 is an undifferentiable zone.

The A horizon in Figure 3 was differentiated into zones I and II. Atterberg limits and bulk density increased with depth. As clay content increased, percent sand decreased. Silt fractions showed a slight increase. The activity of the soil and the moisture content also increased with depth. Sediment was dark gray. Individually, each soil zone shows unique characteristics. Zone I is the till zone, which is vulnerable to disturbance within the soil profile. During the growing season, it represents the dominant crop root depth. Soil moisture was generally low within this zone. However, it is susceptible to rapid increases in moisture content during rainfall events. Zone II constitutes the dominant region of shrinkage cracks, and slickensides, assessed to have the highest activity. According to Klich et al., (1990), the presence of slickensides and cracks are indicators of shear failure in East Central Texas. These soils were susceptible to expansion and contraction due to changes in moisture.

The C horizon was a lithologically distinct layer correlated to Zone III. Soil Atterberg limits and bulk density were higher, the latter of which was measured higher than

the previous zone. Clay content increased as the percent sand and silt decreased. Soil moisture was highest. However, the activity of the soil was similar to Zone I. Sediment was mostly orange-yellow; although a distinct alternation of light gray and yellow banding was observed at the base. Zone III represents the end of the A horizon and the transition zone to the Taylor Marl.

Zone IV was recognized for simplicity as a D horizon. Trends similar to the C horizon continued. Clay content peaked, while sand content was negligible. Despite the generally high silt content within the soil series, silt content was at its lowest, a 10% decline from Zone III. Soil activity was also at its lowest. This zone represents a weathered shale unit basal to the transition zone.

1.1.5 Vertisol Cracking

Soil cracking is a distinctive quality in expansive soils, largely influenced by the impact of climate. Within the Black-Land Prairies, Vertisol cracking is dependent on short and long-term moisture changes (Kishné et al., 2012) and moisture gradients (Wilding et al., 1991) within the soil profile. Recurring periods of wetting and drying and the antecedent water content show positive correlations with crack densities (Kishné et al., 2010; Miller et al., 2010). Further, increases in crack densities within Black-land Vertisols were found to decrease soil water and runoff (Arnold et al., 2005a) . Figure 4 exemplifies the seasonal changes in cracking over a two-year period derived from Arnold et al., (2005a). The figure shows that cracking peaks during the summer months as soil moisture decreases. As moisture increases during fall and winter, soil cracking decreases. According to Arnold et al., (2005a), runoff varies due to changes in soil storage and porosity as cracks contract and expand. This leads to greater infiltration.

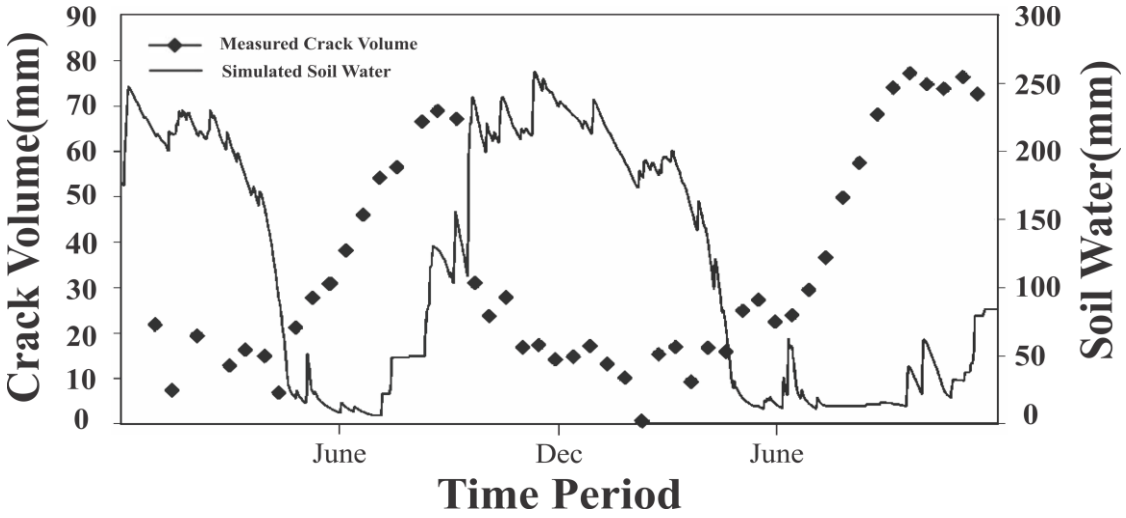

Figure 4: Temporal variability in cracking based on the work of Arnold et al. (2005) for 1998 & 1999.

1.1.6 Site Suitability

The study area contained gullies typical of those seen within the Black-Land Prairies. Google Earth imagery showed the formation of a permanent gully network and adjacent valley side gullies. The history of erosion is tied to the growth of agriculture, urbanization, and terracing. The study area is under seasonal corn cultivation, impacted by terracing and a degrading stream.

The early history of the Black-Land Prairies described in the literature shows a change from native vegetation to agriculture. During European settlement, lands supported tallgrass prairies. Plant species such as big and little bluestem were prevalent (Diamond and Smeins, 1993). However, plowing and mechanized agriculture during the late 19th to early to mid-20th centuries incentivized the removal of climax vegetation (Riskind and Collins, 1975). Corn, wheat, cotton, sorghum, and hay were grown at intervals during agriculture's rise to prominence. The Great Depression of the 1930s fostered a change from mono-crops of cotton to rotational and diverse cropping management strategies. Spurred

on by the hardships of the depression, the land was burdened by the need to increase cotton production for which the prevailing philosophy to overcome financial ruin was to work the land more intensively (Ozment, 1993). Post-1940s, pasture and crops such corn, wheat, and sorghum increased in share as a percentage of cropland and total acreage cultivated (Bland and Jones, 1993).

Post-1950s urbanization accompanied the need to find new and more easily potable forms of water. The use of surface water became prevalent. Various plans and programs were implemented to divert water between basins and reservoirs in the State, raising concerns of bank erosion (F. Yelderman, 1993). Combined with the economic and geotechnical costs of urbanization (Allen & Maier, 1993), channels became susceptible to failure. Urbanization and land management changes were shown to be significant factors leading to increased runoff (Allen & Maier 1993; Harmel et al., 2006), degradation, soil loss, and decreases in soil productivity (Thompson, 1993; Richardson, 1993).

Remedies to combat erosion such as terracing have not always been successful, partly attributed to the sporadic implementation of those measures. Aerial imagery shows channelized erosion within low-lying regions of farms, often at the mouths of terraces, and along stream banks adjacent to Brookeen Creek. For a 10 km^2 area of interest, this trend was validated using LIDAR data (1 m). Arc Hydro point-flow simulations (Maidment, 2002) show that flow concentrates at gully heads within terraces. For the period 1958-1991, Chintala & Allen (1996) estimated vertical incision of 2.1 m, widening to 9.1 m and decreases in the width-depth ratios of the Creek. A comparison of the current channel slope and the equilibrium slope estimated by Chintala & Allen (1996) showed that the channel was degrading and widening. Stages III and IV of the channel evolution model described

by Simon & Rinaldi (2013) represent the current condition. During these stages, degradation leads to bank failure by mass failures and toe erosion when channels exceed their critical height. A network of gullies formed because of the headward migration of knickpoints from the degraded channel. The gully moved along a highway swale and then bifurcated at terrace outfalls.

1.2 Methods

1.2.1 Weather Monitoring

Relationships between precipitation characteristics, drying days and gully migration were evaluated. Rainfall was measured using a tipping bucket rain gauge (Figure 5) based on Brakensiek & Osborn (1979). One rain gauge was mounted on a platform, approximately 0.3 m above the banks, with an Onset H07 data logger. Rainfall was discretized into 10-minute intervals using HOBOware Pro©. The effect of rainfall intensity, number of events and the interoccurrence intervals were further evaluated from precipitation data. Drying days was estimated as the number of days between events. For evaluating the number of rainfall events and interoccurrence intervals, a 10-mm daily rainfall threshold was used. Works by Asquith & Roussel, (2003), Bull (1997), and Vanmaercke et al., (2016) show that rainfall greater than 12.7 mm day^{-1} is a typical rainfall proxy used in the South-western US, and within gully models in North America. Ten-mm was used because it was a similar threshold, and was the most common inter-precipitation event that captured the frequency of storms during field precipitation monitoring (Figure 2). Rainfall intensity was assessed on an event basis in mm hr^{-1} by dividing rainfall totals by the duration of storm events.

1.2.2 Hydrology

1.2.2.1 Moisture. Vertical changes in moisture were assessed at the headcut and banks of the gully. Three Decagon GS3 moisture (± 3%), temperature (± 1º C), and electrical conductivity (± 5%) sensors were used. Measurements were made at the top, middle and lower halves of the gully scarp at about 0.1, 0.4 and 1.1 m below the soil surface. Due to the high shear strength of cohesive soils, moisture probes were installed at the headcut after a rainfall event. Three holes of approximate width to the moisture sensor head were bored into the headcut at each soil elevation so that moisture readings measured would be representative of an unweathered surface. This also mitigated the potential for probes losing soil contact. A three-pronged pin was constructed with a diameter slightly smaller than the probes and inserted into the boreholes to create a cavity that fitted the soil moisture sensors. The pins were made smaller to accentuate soil contact when the sensors were added, thus minimizing disturbance.

Soil moisture was also measured adjacent to the headcut along the left bank using two Delta T ML2 Theta probes (± 1%) with Dynamax loggers at the top and mid banks, about 0.2 and 0.5 m from the bank top. At the right bank, moisture was assessed at the top, middle, and lower banks using the Decagon moisture probes.

1.2.2.2 Discharge. Discharge was assessed using a 2.5-ft H-Flume (Figure 5), constructed using design specifications from Brakensiek & Osborn (1979). The flume walls were fitted into the banks to minimize seepage. A trench was dug 0.6 m from the rear of the flume. One end of a tarp was buried in the trench and the other bonded to the rear of the flume. This was done to mitigate downcutting and water loss at the flume base. Water

levels were logged at 10-minute intervals using a 5 ft, Solinst Level logger pressure transducer (0.05% FS accuracy, ± 1-minute yr^{-1}), housed in a stilling well that was mounted onto the flume sidewall. Barometric pressure was measured using an Onset HOBO Smart Barometric Pressure Sensor CM50 (± 3 millibar accuracy), connected to a HOBO Micro Station Data Logger (± 5-second accuracy per week). A logging interval of 10 minutes was also used. Barometric pressure was subtracted from the transducer head measurements for each storm to compensate for atmospheric pressure fluctuations. Discharge was estimated using a curve fitting equation (± 1.5%) based on the flume rating table.

A Time-lapse camera (Moultrie Wingscape Pro Digital Wildlife) was also installed 1.5 m from the flume to observe changes in the morphology of the headcut, and to compare transducer water levels to surface water elevations. Time-series photos were used as a backup with a staff gauge and rating curve to estimate peak discharge during events where there was undercutting.

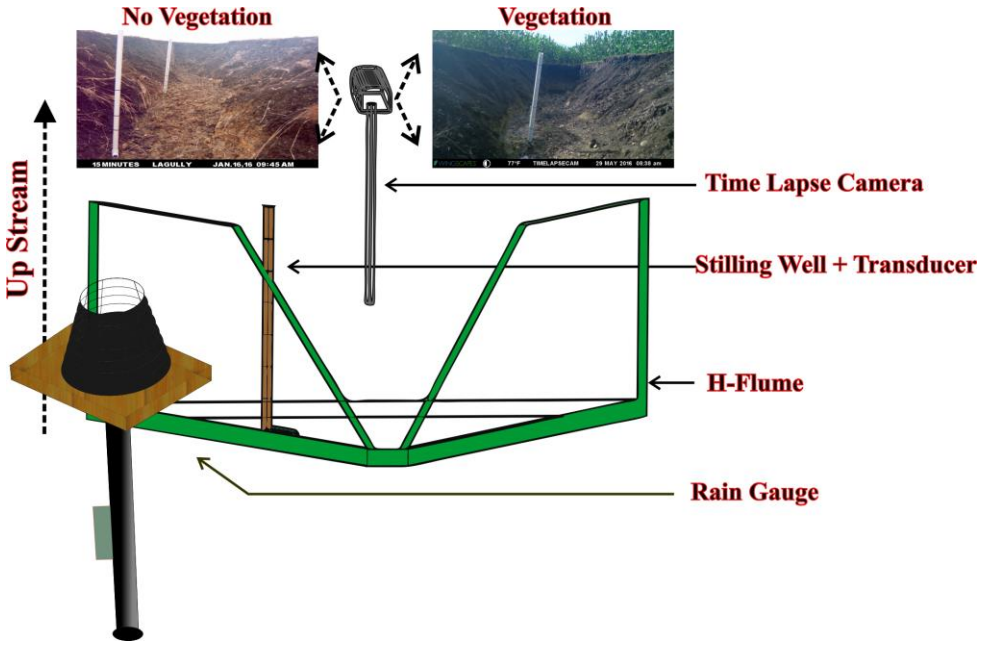

Figure 5: Set up of rain gauge, H-Flume and time-lapse camera for tributary 1. "Vegetation" and "No Vegetation" conditions are shown. A stage recorder was placed 2 m from the rear of the flume.

1.2.3 Soil Properties

The resistance of soils to concentrated flow erosion depends on several parameters, which often show co-dependent relationships. Resistance to erosion is influenced by in-situ soil conditions and external forces impacting the soil condition (Knapen et al., 2007). For cohesive soils, Shan et al., (2015) identified several factors impacting erodibility. However, based on the delineation used by Grabowski et al., (2011), relationships between primary physical soil properties have been explored. Three properties were assessed: Atterberg limits, soil texture, and bulk density.

1.2.3.1 Texture. Soil texture is a surrogate for strength. Fine-grained soils exhibit greater cohesive strength than coarse soils (USDA, 2012). As such, a systematic textural assessment of the gully head and side slope was done vertically. Two grab samples were collected at each sampling elevation. Additionally, estimates of the bed sediment entrained during a typical storm were assessed by digging a trench about 1.5 m from the headcut and installing a bed load container into the trench. All samples were processed in triplicate using the Master Sizer 2000 Malvern laser sampler with the Hydro 2000 MU dispersion unit, and the final grain size results were averaged.

1.2.3.2 Bulk Density. Bulk density was estimated using standard field and laboratory procedures by the United States Department of Agriculture (USDA, 1999). Representative core samples of the banks and headcut were collected in duplicate using a slide hammer and antecedent moisture cores. Sampling was done toward the end of the investigation period to minimize disturbance at the headcut.

1.2.3.3 Consistency (Atterbergs limits). Atterberg limits express consistency boundaries that qualitatively define the behavior of cohesive soils at different moisture conditions. Most important are the plastic limits and liquid limits. Studies have shown that these limits are important soil factors related to soil moisture and strength in cohesive soils (Widodo et al., 2012; Vardanega and Haigh, 2014). Grab samples for Atterberg limit testing were collected methodically down the gully side slope. Samples were sent to TRI Geotechnical Inc for Atterberg testing (ASTM standard D4318).

1.2.4 Migration

1.2.4.1 Geographic positioning systems (GPS). GPS has been effective in gully erosion studies (Nazari Samani et al., 2009; Frankl et al., 2012), permitting post-processing of data using geographical information systems (GIS). GPS techniques were used for monitoring changes in gully morphology at the headcut, channel, and overbank. For improved surveying accuracy, a Trimble R8 GNSS Kinematic GPS with cm RTK accuracy was used according to manufacturer specific usage and surveying guidelines (Trimble Navigation, 2003). Measurements were taken using an occupation time of 3 seconds, and the data projected in the Texas Central 4203 (US State Plane 1983) spatial coordinate system in Lambert Conformal Conic projection. GPS was used for this investigation because of the high accuracy of Kinematic GPS, and the absence of trees and other structures that may contribute to signal interference and multipath errors. These uncertainties associated with GPS methods are limited in an open farm field. As such, dilution of precision due to ambient orientation and the roving station environment of the receiver during data collection was minimized.

A survey of the gully network (periphery and channel) was conducted at the start of the monitoring period (October 2015). Time-lapse GPS measurements were taken after storms starting in February 2016. Tributary 1 was the primary gully monitored, while tributaries 2 and 3 were observed less frequently to compare extension rates in Figure 1. Waypoints were collected above and along the perimeter of the head-scarp. These points were imported into ArcGIS Professional©, where a digitized line segment representative of the form of the headcut was drawn to delineate the headcut position after each storm event. The headcut extension was calculated as the distance between those points.

1.2.4.2 Erosion pins. Erosion pin methods (Bartley et al., 2007; Ghimire et al., 2013) were used to verify the accuracy of headcut extension data at Tributary 1. A network of 9 pins was used to estimate sidewall and headcut erosion. The method was later discontinued to mitigate some of the uncertainties identified by Boix-Fayos et al., (2006) in erosion studies, e.g., the disturbance of soil layers. Kinematic GPS waypoints avoided some of these uncertainties, and allowed for a better representation of the headcut morphology because of the ability to acquire more data points above the gully head in less time. The erosion pin method more frequently underestimated migration rates during periods of greater headcut extension. Potentially, movement of pins during more erosive flows could have contributed to this. Additionally, erosion pin methods were used to estimate changes in bed elevation. Pins were installed in pairs along the channel.

1.2.4.3 Structure-from-motion. Structure-from-motion (SFM) (Ullman, 1979) and integrated multi-view approaches are new technological advances that are increasingly used in geomorphic change applications (Snavely et al., 2006; James & Robson, 2012).

The methods have found increasing utility in gully erosion studies (Gómez-Gutiérrez et al., 2014; Castillo et al. 2012; Marzolff & Poesen, 2009) proving an invaluable additive tool to more traditionally established methods such as LIDAR (James et al. 2007), aerial photos (Daggupati et al., 2014) and interviews (Nyssen et al., 2006). Castillo et al., (2012) demonstrated the accuracy and cost-time benefit of various 3D (LIDAR, 3D Photo Reconstruction) and 2D (Total Station, Profile Meter) methods in gully volumetrics, showing greater comparative accuracy for photo reconstruction methods.

SFM entails the identification of matching points within images taken in obliquity and the use of algorithms for photo reconstruction. The scale-invariant feature transform (SIFT) algorithm is typical (Lowe, 2004). SFM was used to capture time-lapse morphological transitions of the gully headcut and volumetric changes. Three software packages were used for data processing and visualization: Agisoft PhotoScan Professional© (Agisoft LLC, 2017), Cloud Compare© (DGM et al., 2017), and ArcGIS Professional©. Data collection and processing were done using an analogous workflow to Kaiser et al., (2014), and Prosdocimi et al., (2015) using high-resolution model outputs from PhotoScan. Ground control points were employed for georectification, and volumetric estimates were obtained using ArcGIS. Data were collected and analyzed in two phases using a terrestrial (1st phase) and Unmanned Aerial Vehicular (2nd phase) application of the SFM method.

Time-lapse headcut morphometric changes of the gully head were captured during the first phase. Tributary 1 (Figure 1) was the only gully evaluated. The generalized workflow is depicted in Figure 6, over a 7-month monitoring period. In this study, benchmarks were set at key locations along the gully head and a Trimble R8 GNSS.

Kinematic GPS was used for ground control (Figure 6:1). Benchmarks were additionally placed in regions outside of scene vanishing points to enhance model feature distances and to minimize nonlinear structural errors (Westoby et al., 2012). Three different cameras were used: Samsung G386T (5 MP), Konica Minolta Dimage G600 (6 MP), and an Olympus Stylus Touch TG4 (16 MP). Focal lengths of 3 mm (1280 ×720) pixels, 8 mm (2272 ×1704) and 4mm (4608 ×3456) pixels were used for image capture, respectively.

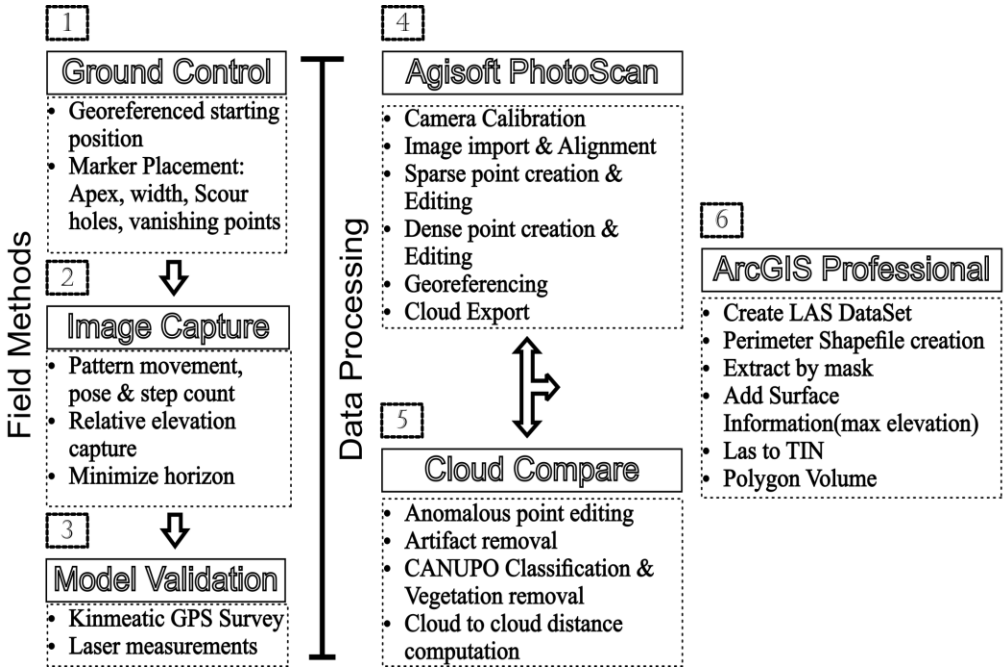

Figure 6: Generalized Structure from Motion (SFM) field and data processing workflow for data capture phases.

Images were captured at the bank top and within the channel at a maximum distance of about 6 m (Figure 6:2). Increased proximity to the headcut can be expected to produce increased point densities in the priority areas (head scarp). Two relative elevations were used for image capture at the bank top while moving along the perimeter with an approximate 45º point of view (POV). A multi-view approach offers good depth perception. At least three benchmarks were captured in each image, and two pictures were

taken at each point along the apex perimeter. Images were taken to minimize the appearance of the horizon, thereby decreasing the post-processing time of artifacts in Photo Scan.

Figure 6: 4,5,6 catalogs the post-processing procedures. In the CloudCompare© data processing phase, the use of the 3D trained classification scheme (Brodu & Lague, 2012), incorporated as the CANUPO plugin was not done to classify vegetation because there was none. In step 6, a time series analysis of the volumetric retreat rate was conducted by modifying the generalized process (Figure 6:6). LAS datasets were converted to digital elevation models (DEMs), sampled to the accuracy of the Kinematic GPS (5 cm). A digitized reference line was set based on the first SFM data set. The resulting data set was then merged with the first, and the volumetric change estimated as the difference between merged and initial triangular irregular networks. This was repeated for succeeding DEMs.

A summary of the unprocessed model statistics from AgiSoft© is presented in Table 2. Using 10 control points, Gómez-Gutiérrez et al., (2014) found root mean square errors using 123D catch comparable to those presented. Maximum point-cloud densities of 2 points cm^{-2} were reported. In this study, point densities range from 4-30 points cm^{-2} (Table 2). The detail of the models was considered adequate for further analysis due to the scale and objectives of the study. For SFM techniques, well-exposed photographs of the area of interest are considered to be the main requirement for photo reconstruction (Westoby et al., 2012; Prosdocimi et al., 2015). Moreover, the flexibility of the processing software, and the precision of the instrumentation minimizes the potential uncertainty associated with variable camera parameters. Cameras were calibrated using Agisoft Lens

before model development in PhotoScan, and headcut measurements were taken with a hand-held laser for verification.

The use of Unmanned aerial vehicles (UAV) in soil erosion applications is a recent advance in the field of geomorphology, facilitating change detection on a larger scale compared to the terrestrial method used above. Detailed 3D models can be obtained with high spatial (cm accuracy) and temporal resolution (Tonkin et al., 2014; Wang et al., 2016). Data acquired have the added advantage of repeatability when benchmarks are surveyed into terrain models.

Table 2: Digital elevation model statistics (GC: ground control, PD: Point Density, RES: resolution)

Model	GC RMSE (cm)	PD (Points cm^{-2})	Res (mm pix^{-1})	Camera Model
1	2	26	3	Konica Minolta Dimage
2	3	12	3	Olympus Stylus Touch
3	9	4	5	Samsung G386T
4	3	30	2	Konica Minolta Dimage

$$\Delta V = TIN_{SFM} - TIN_{LIDAR} \quad (1)$$

where ΔV is the change in gully volume; TIN_{SFM} is the triangular irregular network derived using structure from motion; TIN_{LIDAR} is that derived from LIDAR data.

A DGI Phantom 2 with camera model FC300X (4-mm focal length) and a LIDAR survey (1 m) flown by TNRIS in March of 2013 were used to estimate the volumetric change within tributaries 1,2 and 3 (Figure 1). Data capture took approximately 20 minutes. The application workflow in Figure 6 was used with some notable differences. In the ground control stage, 12 markers were surveyed using the Kinematic GPS. For image capture, a pre-flight plan was programmed for the drone ensuring 60% image overlap. No changes in the workflow for data processing in AgiSoft were required. Structure-from-

motion models were created using the highest resolution in photo scan with 230 photos. In the CloudCompare© data processing phase, the CANUPO plugin aided in the removal of vegetation in tributary 3. The classification was done balancing the need for a clean data set and maintaining the topological integrity of the terrain. Differences in gully volumes (ΔV) were estimated using triangular irregular networks (TIN) of the SFM and LIDAR LAS datasets by (1).

1.3 Results

1.3.1 Water Balance for Study Period

1.3.1.1 Precipitation-moisture variability Precipitation and soil moisture are interrelated parameters that influence the catchment response to rainfall. Precipitation is the input to the system, while the initial soil moisture impacts runoff and infiltration. Changes in soil moisture are temporal and spatial. According to Fitzjohn et al., (1998), the temporal variability may be useful in predicting wetness thresholds for runoff, while the spatial variability depicts regions of differing hydrologic response. Soil moisture is also an important factor impacting cohesion in clays, which according to Vanmaercke et al., (2016) might be the most important soil property impacting headcut retreat. Moisture is also related to soil plasticity, cracking, shear strength, compaction and bulk density (Knapen et al., 2007).

$$API_t=(API_i)(K)^t \quad (2)$$

where API_t (mm) is the evaluated API after t days, API_i (mm) is the initial API , and K is a unitless decay coefficient

The temporal variability in soil moisture for the entire monitoring period was evaluated using the Antecedent Precipitation Index (API) (Smith & Welborn, 1967). API is a lumped parameter based on rainfall, derived from inter-dependent variables which influence soil moisture before a storm, e.g., evapotranspiration and runoff (Smith & Welborn, 1967). The API used was developed at Pin Oak Creek in the southeast corridor of Hill County, a distance of 24 km from the study area (Figure 1). Land use, rainfall, geology, and soils were considered sufficiently similar to justify the application of this model. As such, the decay coefficient (0.92) by Smith & Welborn, (1967) was used. The API was estimated using measured rainfall during the observation period by (2).

API and rainfall statistics were used to assess soil moisture during the monitoring period. The relationship between API and rainfall is shown in Figure 7, while Table 3 summarizes the corresponding API statistics. Soil moisture was evaluated from API measurements based on the correlation of the API model with moisture evaluations within Zone I (Figure 3) at the site. Daily moisture was assessed continuously for the periods labeled M_1-M_4 on Figure 7 at a depth of approximately 20 cm from the soil surface. These moisture measurements spanned for periods of 7, 11, 4 and 1 day. Within the Black-Land Prairies, Smith & Welborn, (1967) found that an API of 177 mm or above represents saturated conditions. One peak exceeded this value with an additional 4 peaks near an API of 155 mm. The average API was 63 mm.

Figure 7 depicts three different precipitation distributions labeled as periods 1,2, and 3. These periods were subdivided based on storm intensity and frequency. Listed in Table 3, are storm characteristics for the various periods. Period 1 saw high intensity-low frequency storms. The average interoccurrence period was 10 days, with a total of 426 mm

of rain. During the second period, rainfall totals were at their highest, while the interoccurrence period decreased by half. The average daily rainfall was greater for period 2. Period 3 was marked by the lowest rainfall totals, an increase in the average storm intensity, and the greatest storm interoccurrence period.

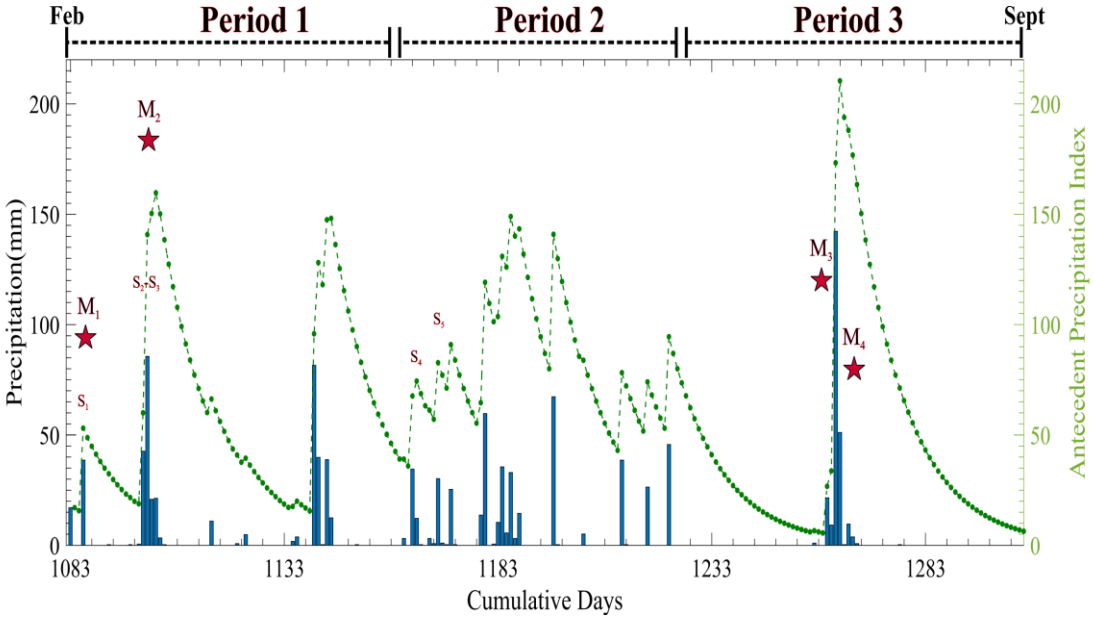

Figure 7: Temporal variability in soil moisture using the Antecedent Precipitation Index (API) for the field monitoring period.

Table 3: Descriptive statistics for API during field monitoring. Rainfall intensity and the inter-occurrence periods represent average daily values.

Period	Precipitation Statistics (mm)			API Statistics (mm)			
	Total	Intensity (day^{-1})	Inter-Occurrence Interval (days)	Average	Minimum	Maximum	Standard Deviation
1	426	19	10	63	15	160	48
2	470	17	5	81	35	149	28
3	240	24	24	46	5	210	52

The predicted API varied with the precipitation distributions. The standard deviation was used as an indicator of variability. Table 3 shows that API fluctuated rapidly during period 1. The average API was 63 mm, with a minimum and maximum of 15 and

160 mm. The variability in API was 48 mm. Period 2 saw a higher but more consistent API. An average of 81 mm was estimated, with a variability of 28 mm. During period 3, the average API was lowest. The API also reached its minimum (5mm) and maximum (210mm) points during the monitoring period.

$$M_{soil} = (API)\ (0.12) + 27 \quad (3)$$

where M_{soil} is the soil moisture based on API

RHS constants vary between (0.09) : (0.16) and (23.5) : (30.5) at the 95% confidence interval

The relationship between API and measured soil moisture was evaluated to validate its use as a predictor of soil moisture changes, and to provide a method for estimating temporal changes in volumetric water content. Figure 8 depicts this relationship. An R^2 of 0.72 was obtained based on (3). The variability in the constants for the linear equation is also shown, allowing for maximum and minimum assessments of soil moisture. Field capacity and saturation for the soil zone are shown in Figure 8 based on estimates from Saxton & Rawls (2006). A normally compacted soil having 1.5% organic matter and a salinity of 1.0 dS m^{-1} is saturated at 46% volumetric water content. Field capacity occurs at 33%, while the wilting point is 16%.

During the observation period, soil moisture was generally at or above field capacity, varying between wilting point and saturation. Figure 8 shows that saturation occurs at an API of 155 mm. This differs from the findings of Smith & Welborn, (1967) who predicted 177 mm at Pin Oak Creek. Field capacity occurs at approximately 50 mm, while wilting point occurs at about 5 mm. The API model suggests that soil moisture reached saturation during all three precipitation periods. Period 3 (Figure 7) saw the

greatest variability in soil moisture. Moisture approached wilting point and exceeded field saturation within the period.

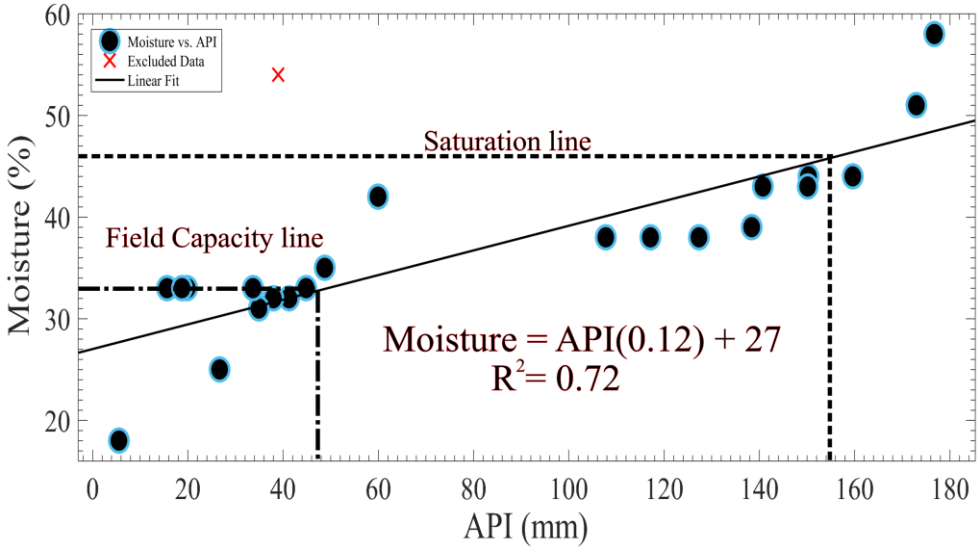

Figure 8: relationship between API and soil moisture at tributary 1.

Moisture readings were sensitive to rainfall frequency and magnitude. At M_1 and M_3 (Figure 7), low-intensity storms generally produced greater moisture increases. However, high-intensity storms (M_2) had the opposite effect. Controlling for this variability, one point shown in Figure 8 was excluded from the regression. Based on the moisture response at similar API's, the point was thought to be anomalous. However, if this datum is included, the adjusted regression coefficient was 0.52.

1.3.1.2 Run-off-infiltration variability. Changes in runoff within Black-Land Prairie Vertisols are related to precipitation characteristics and the initial soil moisture. Four soil water phases are described by Allen et al., (2005), influencing runoff. Based on long-term evaluations by Harmel et al.; (2006), these phases fall into "dry," "field capacity," "saturated" and "transition periods." The dry period occurs from July to September. Runoff is limited, and soil cracking is greatest, partly attributed to high summer temperature and

drier summer soils. Field capacity occurs from December to January where runoff increases due to increased rainfall and lower evapotranspiration. The saturated period occurs from February to May during which runoff peaks because of more rainfall. May to June represents the transition period where cracks reopen and evapotranspiration increases. Runoff typically decreases.

Runoff and infiltration were assessed using discharge estimates at the gully head of tributary 1, based on the H-Flume set up shown in Figure 5. Five storm events were chosen for analysis after correlating the flow depth from the stage recorder with the transducer head measurements. Table 4 lists the rainfall inputs, average flume readings and estimates of runoff, lag time, and infiltration for each storm. For simplification, the end of a storm event was taken as a zero transducer head reading, although low flows were observed after transducer readings ceased. For runoff estimates, it was assumed that the entire drainage basin of tributary 1 was the contributing catchment. Infiltration was estimated as the difference between rainfall totals and runoff, while lag times were assessed from time-lapse observations of storm events.

The storm events shown in Table 4 occurred under different growing conditions. Of the 5 storms, storms 1-3 occurred on uncultivated terrain, while storms 4-5 occurred during the cropping period. For comparison to Figure 7, the first 3 storms occurred during period 1, labeled as S_1 to S_3. The last 2 occurred during period 2, labeled as S_4 and S_5. Storms 2 and 3 occurred within the same storm cycle. It is notable that runoff and discharge for storm 3 are likely greater because repairs were done to the flume after this storm due to high flows and sedimentation. Subsequent comparisons are only made to show the minimum change in the runoff magnitude for concurrent storm events. However, Table 4

summarizes that runoff was greater during the uncultivated period. Moreover, infiltration estimates were generally constant during the uncultivated period, but showed greater variability during the cropping period.

Table 4: Storm characteristics for five recorded storm events based on rainfall totals. Average values are shown for rainfall intensity and flume outputs.

	Rainfall Input			Average Flume Output		Waterhshed Estimate		
Storm	Inter-Occurrence Interval (days)	Rainfall (mm)	Intensity (mm hr^{-1})	Head(m)	Discharge (m^3s^{-1})	Lag Time (min)	Runoff (mm)	Infiltration (mm)
1	2	38	8.3	0.03	0.001	190	1.5	36.5
2	13	41	49.1	0.04	0.003	40	5.2	35.8
3	0	62	9.7	0.10	0.015	10	8.4	53.6
4	18	47	6.8	0.04	0.002	380	1.3	45.7
5	4	30	14.5	0.09	0.008	30	2.4	27.6

Table 4 also shows significant variability in flume outputs and watershed estimates on an event basis. Outputs varied with rainfall intensity and the storm interoccurrence periods. Storm discharge and flow depth increased with rainfall intensity and fewer interoccurrence days. Runoff estimates also increased. The greatest change in runoff occurs for succeeding events, e.g., storm 3 where the average discharge increased by a factor of 5.

To further evaluate rainfall, runoff and infiltration characteristics, the Green & Ampt method for unsteady rainfall (Mein & Larson, 1973; Chu, 1978) was implemented. The model simulates ideal conditions for estimating infiltration and runoff using break-point rainfall. Green & Ampt theorizes that infiltration occurs if the rainfall intensity is less than the saturated conductivity, or if the intensity is greater than the saturated conductivity but less than the infiltration capacity. During the latter, moisture increases within the soil profile (Mein and Larson, 1973). The method was amended by Chu, (1978) to accommodate unsteady rainfall by introducing a ponding time and a pseudo-time factor.

Work by Lepore et al., (2009) suggests that the method may be inadequate for predicting runoff for clay-rich soils, which are prone to cracking and preferential flow. However, due to the impact of rainfall characteristics on runoff, the Green & Ampt method was used as a framework for estimating the catchment response to variable rainfall. An additional outcome of this investigation is the ability to compare runoff with the API and moisture assessments from Figure 7.

The Green & Ampt model was calibrated to cumulative runoff for each of the 5 storm events listed in Table 4. Table 5 lists the calibrated model parameters and the simulated runoff outputs. Rainfall was discretized into 30-minute intervals for use in the model. The saturated water content (VWC_{Sat}) was estimated at the liquid limit, with the initial moisture (VWc_{Ini}) set from field data. Soil textural characteristics based on Rawls et al., (1983) were used to constrain soil suction, varying between 189 mm and 635 mm. High suction (510 mm) and low surface storage (1 mm) offered the best calibration of the data. Each storm event was successively calibrated to the observed runoff values listed in Table 4 by adjusting the vertical saturated conductivity (V_{Sat}), and finely adjusting other parameters. An average V_{Sat} of 0.9 mm hr^{-1} (0.9 mm stdv) and infiltration rate of 5.7 mm h^{-1} were predicted. The average calibrated conductivity estimate was comparable to evaluations by the USDA (NRCS, 2017) (0.75 mm h^{-1}), and Rawls et al., (1983) (0.65 mm h^{-1}). Observed (Table 4) and predicted (Table 5) runoff estimates showed reasonable fit, with absolute residuals of less than 0.3 mm for storms 1,3,4 and 5. Storm 2 was exceptional. The model underpredicted run-off by 1.2 mm.

Table 5: Green & Ampt calibration for the storm events shown in Table 4. VWC_{Ini} is the initial water content; VWC_{Sat} is the saturated water content; Suction is the average value across wetting front; V_{Sat} is the vertical saturated conductivity; Surface storage is the maximum value over the watershed.

Storm	Adjusted Model Parameters					Model Output
	VWC_{Ini} (%)	VWC_{Sat} (%)	Suction (mm)	Surface Storage (mm)	V_{Sat} (mm hr^{-1})	Runoff (mm)
1	33	53	510	1	1.2	1.79
2	33	53	500	1	0.0001	4.00
3	52	53	510	1	0.0001	8.34
4	33	53	510	1	1.1	1.40
5	33	53	510	1	2.2	2.70

The Green & Ampt method generally overpredicted runoff and underpredicted infiltration during continuous simulation, with the effect increasing for lower storm interoccurrence intervals. Figure 9A shows the model run based on the average calibrated parameters listed in Table 5, called the initial calibration. Model runs were done on an hourly time step and summed up as daily values of infiltration and runoff. The figure also shows the potential uncertainty in runoff as error bars, estimated using the root mean square error (RMSE). In Figure 9A, RMSE was estimated at 22 mm. The average runoff and infiltration were 15.5 and 4.2 mm.

Runoff was adjusted using the precipitation to runoff ratios from Table 4. The excess runoff was linearly added as infiltration to the post model calibration. Adjustments were made to include the change in the precipitation to runoff ratios for the cropping and uncultivated periods. Figure 9B depicts the model simulation incorporating these ratios which are based on observed data, here called the adjusted calibration. The RMSE was estimated at 1 mm, while the average runoff and infiltration was 5.2 and 14.5 mm, respectively.

Clearly, the adjusted calibration carries a lower degree of uncertainty, observed as a decrease in the RMSE, and better comparative accuracy to measured runoff values listed in Table 4. In Figure 9A, runoff residuals of 7.5, 13.8, 2 and 14.5 mm were estimated for events 1, 2, 4 and 5 respectively. The adjusted calibration produced residuals of 1.3, 1.3, 1.9, and 0.6 mm. The need to further improve the calibration was related to the inability to parameterize land-use changes and crack flow during continuous simulation, the latter of which Arnold et al., (2005) estimates to be a significant contributor to changes in runoff within the Black-Land Prairies.

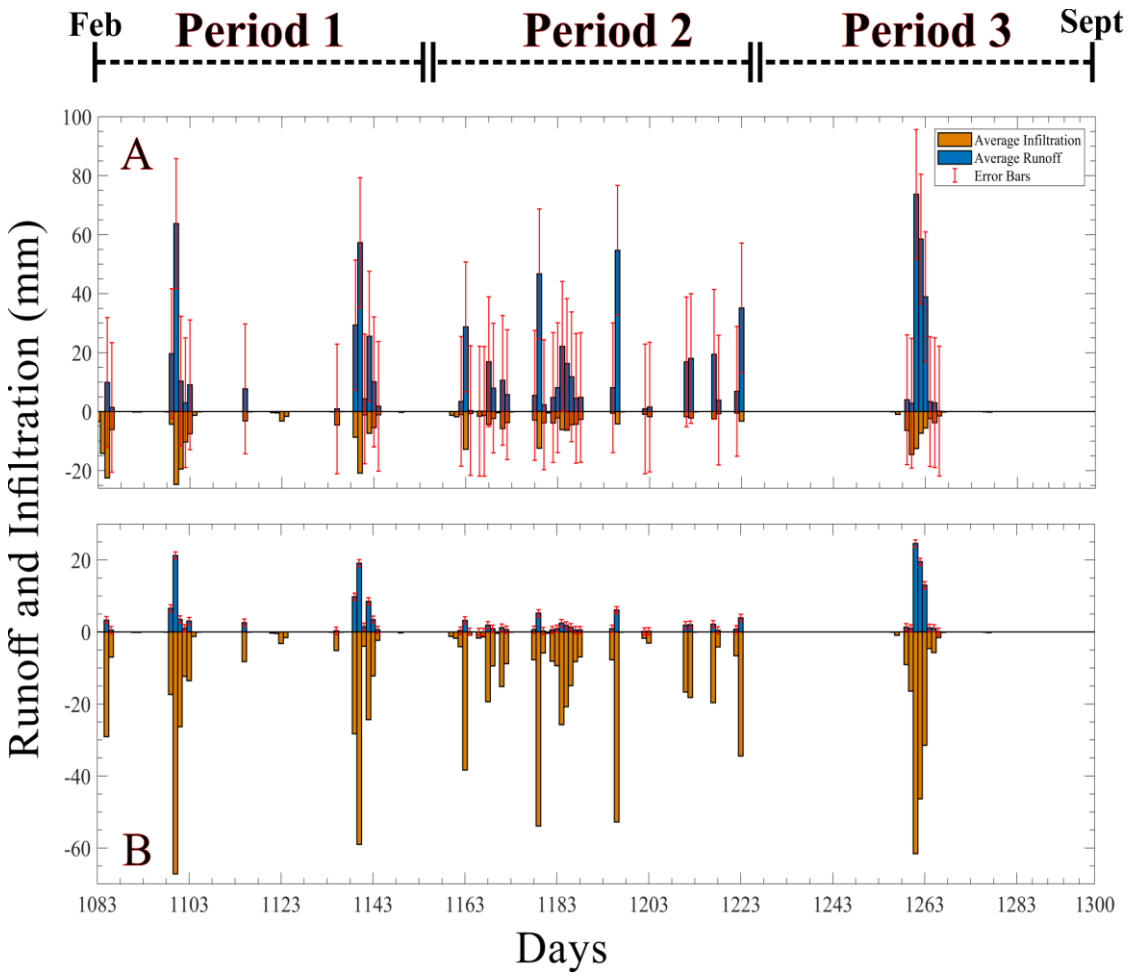

Figure 9: Green & Ampt calibrated model runs. (A) Initial Calibration (B) Adjusted Calibration

The precipitation-runoff response was generally flashy, a term used by Poff et al., (1997) to explain the variable rate at which flow changes within rivers. This finding agrees with time-lapse observations of storms, particularly during wet phases of the monitoring period. A short duration rainfall event on day 1100 presents such an example. Thirteen mm of rainfall produced a flow depth of 0.15 m, and peak discharge of 0.016 $m^3 s^{-1}$, which was atypical of the precipitation magnitude. This is related to the variable lag observed for storm events, which based on Table 4 is correlated negatively to storm intensity and positively to storm interoccurrence intervals. Moreover, lag times varied with growing conditions, increasing during the cultivated period.

1.3.2 Headcut Retreat and Soil Loss Relationships

The retreat of headcuts is related to the height of the scarp (Robinson & Hanson, 1995a; Bennett & Casalí 2001; Vandekerckhove et al. 2003; Hanson et al. 2001). While height is a simple geometric property of the scarp impacting flow at the overfall, and can be quickly measured in the field, migration predictions based on scarp height show variability for smaller changes in elevation, as in Bennett & Casalí (2001) ($R \approx 0.55$). Work by Robinson & Hanson (1995a) shows that migration rate shows slight increases when other variables are controlled, such as moisture and density. However, taller headcuts produce more sediment as Bennett & Casalí, (2001) showed, with $R \approx 0.95$. In soils ranging from silty clays to silty clay loams, work by Vandekerckhove et al., (2003) agrees with the significance of the over-fall as an important geometric property explaining volumetric soil loss over medium time scales ($R^2 \approx 0.64$). One plausible explanation for this height induced instability was offered by Hanson et al., (2001), who showed that increasingly positive ratios of headcut height (H) and scarp erosion ($2E_v$) induced failure.

Scarp retreat is also related to the size of the catchment. Many studies have shown a positive correlation between the two parameters (Frankl et al., 2012; Vandekerckhove et al., 2003). However, as headcuts migrate upstream, the basin area decreases. The decrease in catchment size may result in lower migration rates and sediment yield, which was initially proposed by Graf (1977) as the rate law of geomorphology. The rate law describes spatial and temporal adjustments within geomorphic systems occurring to balance disruptions (rainfall and erosion) affecting the equilibrium state of the system.

Over the assessment period, headcut migration generally increased. Migration was assessed using differential GPS, with the erosion-pin method as a backup. Figure 10 depicts linear fits of the changes in migration for the gullies investigated for the entire observation period (Figure 2). R^2 values of 0.99, 0.97, 0.93 and 0.40 were obtained for tributaries 1, 2A, 2B and 3, respectively. RMSE values of 0.2, 0.6, 1.1, and 0.2 m were estimated. Most data points fell within the 95% confidence intervals, shown as dashed red lines (Figure 10). Clearly, tributary 1 showed the greatest change in migration, while tributary 3 showed less movement. Tributary 1 migrated a total distance of 27.7 m, while tributaries 2A, 2B and 3 moved 18.4, 17.5 and 4.2 m, respectively. The spatial differences in migration, and deviations from the confidence intervals suggest that other factors may mechanistically inform migration predictions.

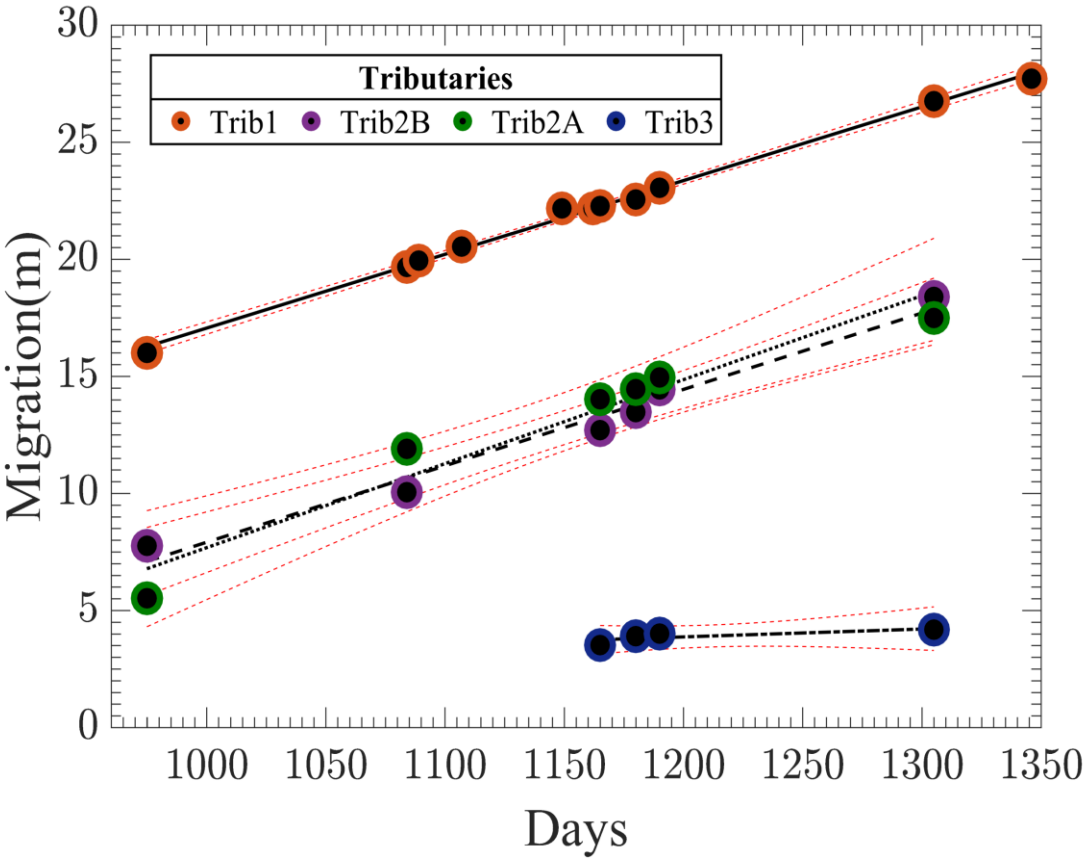

Figure 10*:* Medium-term gully migration trends (3.6 yrs.) for tributaries1-3. Figure 4 was used as the starting date for the evaluation period. Two regressions are depicted for Trib. 2, representing a second-order gully network: T-2A, T2-B based on Figure 1 .

Because of the increase in rainfall over the monitoring interval (Figure 2), migration was evaluated over short and medium-term timescales. Short-term refers to the precipitation monitoring interval (annual time-step), while the medium-term is assessed as the observation period (3.6 years). Table 6 summarizes this comparison. Tributaries 2A and 2B are combined into an average retreat called tributary 2. Short-term migration was greater than medium-term assessments. The greatest difference in retreat rates over the timescales occurred at tributary 2, while the lowest was for tributary 3.

Significant differences in migration rates were observed for medium and short terms. Table 6 demonstrate these differences. For medium-term evaluations, tributary 1

migrated at 1.5 times the rate of tributary 2, while tributary 2 migrated at 4 times the rate of tributary 3. Within the second-order gully network at tributary 2, the rates were similar. During short-term monitoring, tributaries 1 and 2 had similar migration rates, while tributary 2 migrated at 6.7 times the rate of tributary 3. Tributaries 2A migrated faster than 2B.

Table 6: Linear, volumetric and surface area changes over medium and short temporal scales. Volumetric and surface area changes were derived from Lidar and SFM DEM model differences (Figure 2). The medium term refers to a 3.6 yr. period, while short term refers to 1 yr.

Tributaries	Δ Surface Area	Δ Volume	Medium Term Growth (m yr^{-1})	Short Term Growth (m yr^{-1})
1	1119	871	7.5	11.2
2	2597	2449	4.95	11.5
3	215	340	1.2	1.7

Gullies show complex changes in morphology as they migrate and evolve over time. These are related to channel and basin characteristics. Table 7 shows the initial site morphometrics based on the LIDAR dataset. Channel attributes (width, depth) are calculated averages representing the DEM cross-sections taken from the headcut, channel center, and mouth. Channel length was estimated based on a digitized thalweg length profile. The slope was estimated from the same profile. The catchment slope was calculated as the average slope of the delineated catchments (C1-C3) shown in Figure 1.

Table 7: Initial channel and catchment gully morphologic attributes derived from Lidar survey (Figure 2).

	Channel Attributes					Catchment Attributes	
Tributary	**Width (m)**	**Depth (m)**	**Overfall Height (m)**	**Length (m)**	**Slope**	**Slope**	**Area (m^2)**
1	7.3	2	1.1	99.7	0.098	0.045	23060
2A	7.5	1.9	0.9	76.2	0.187	0.044	12784
2B	7	1.9	0.9	93.7	0.176	0.041	14138
3	6.7	1.6	1.0	62.5	0.144	0.049	19001

Individual drainage areas deviated from the expected positive correlation between basin size and migration. The relationship was inconsistent for both timescales investigated (short: medium); tributary 3 with the second largest basin had the lowest migration rate.

Overfall height varied spatially and as the gully head migrated over time. The height was measured as the distance from the brink to the channel bed. In order of decreasing height, tributary 2B was tallest (1.5 m) followed consecutively by tributaries 2A (1.3 m), 1 (1.2 m) and 3 (0.6 m). Tributary 1 deviated in height by about 0.2 m, while tributary 3 showed very little change (stdev ≈ 0.04 m).

The amount of variation in headcut retreat explained by changes in height was weak, an R^2 of 0.3. Height measurements from tributary 1 were used for this evaluation, and varied between 1 and 1.4 meters. As such, the spatial variability in height for tributaries 1 to 2 were similarly considered less significant during retreat. Robinson & Hanson (1995a) found similar uncertainties for changes in height ranging 0.2 m when soil properties varied during investigations. Measurement uncertainties of scarp height in the field, and the accumulation of talus may have contributed to the low significance of the parameter. Further, the headcut showed dynamic changes in morphology as it evolved over time.

Soil loss rates for gullies in Vertisol terrain show significant variability. Loss rates ranging between 1.3 and 425 m^3 yr^{-1} were reported by Frankl et al., (2012); several factors related to drainage area, headcut height, and changes in precipitation patterns affected this distribution. Table 6 lists the changes in gully volume and surface area over the medium term in this study. Soil loss estimates were obtained using the methods outlined in the second phase of the structure-from-motion data capture procedures. Volumetric soil loss was related to the surface area of the gully. Most sediment was lost from the second-order gully network at tributary 2, which cumulatively has the greatest catchment area and surface area. A total of 3665 m^3 of sediment were lost for all tributaries over the medium term, representing a loss rate of about 1018 m^3 yr^{-1}.

Time-lapse estimates of the volumetric changes at tributary 1 were obtained using SFM methods based on the procedures outlined in the first phase of processing. 28 m^3 of soil was lost from day 1149 during short-term evaluations, representing a loss rate of 38 m^3 y^{-1}. If soil loss was estimated as the volumetric differences between consecutive gully heads, a total change of 11 m^3 was assessed. As such, point-to-point changes due to migration contributed slightly less than half the sediment lost at the headcut.

1.3.3 Changes in Headcut Morphology

Several mechanisms for headcut failure and migration have been proposed involving complex processes such as plunge pool erosion (Flores-Cervantes et al., 2006), cantilever failure (Stein and LaTray, 2002) and differential stresses (Collison, 2001). For many retreat models, a homogeneous lithology is often assumed such as done by Alonso et al., (2002), which is reasonable considering lithologic complexity. Often the dynamics of aerated and non-aerated overfalls further differentiate models. Consequently, the

geomorphological changes occurring during headcut evolution have seldom been documented in the field with high fidelity. Processed-based evaluations are often conducted in flumes (Bennett & Casalí, 2001; Bennett et al., 2000; Ploumis-Devick, 1985). A series of papers by Hanson & Robinson, (1993); Robinson & Hanson, (1996), Robinson, (1996), Robinson & Hanson, (1995b), Robinson & Hanson, (1995a), Hanson et al., (2001) demonstrate the complexity of gully advance through evaluations of overfall height, soil type, moisture, and water elevation below or downstream of headcuts (backwater).

$$H_{critical} = \frac{4\,(C)}{\rho_d} \tag{4}$$

where $H_{critical}$ is the critical height, C is soil cohesion and ρ_d is the bulk density

Four growth stages (Figure 11) were identified as the gully head evolved: Initiation, Planform Incision, Expansion, and Stabilization. The growth stages are conceptualized using space for time substitutions, field measurements, site and video observations and structure-from-motion data. The RMSE for the SFM models were listed successively in Table 2. Headcut height was thought to be an important property during the evolution of the gully head because it controls the erosive ability of water flowing at the overfall (Stocking, 1980). The critical height, defined as the maximum height for which a slope is stable under a given set of environmental conditions should represent a distinct moment in the evolution of the headcut. As such, critical height was approximated based on work by Duncan et al., (2014) using minimum factor of safety calculations (FS≈1) for a vertical slope by (4). The factor of safety is the ratio of the available resistance to shear to the resistance needed for equilibrium (US Army Corps of Engineers, 2003). A safety factor of 1 suggests that the slope is stable. Theoretically, FS is inversely related to height. By (4),

$H_{critical}$ is based on cohesion and bulk density. Bulk density was approximated using average values from Figure 3; $H_{critical}$ was estimated at 0.7 m. Generally, headcuts of greater height will be less stable than shorter ones for a given set of environmental conditions.

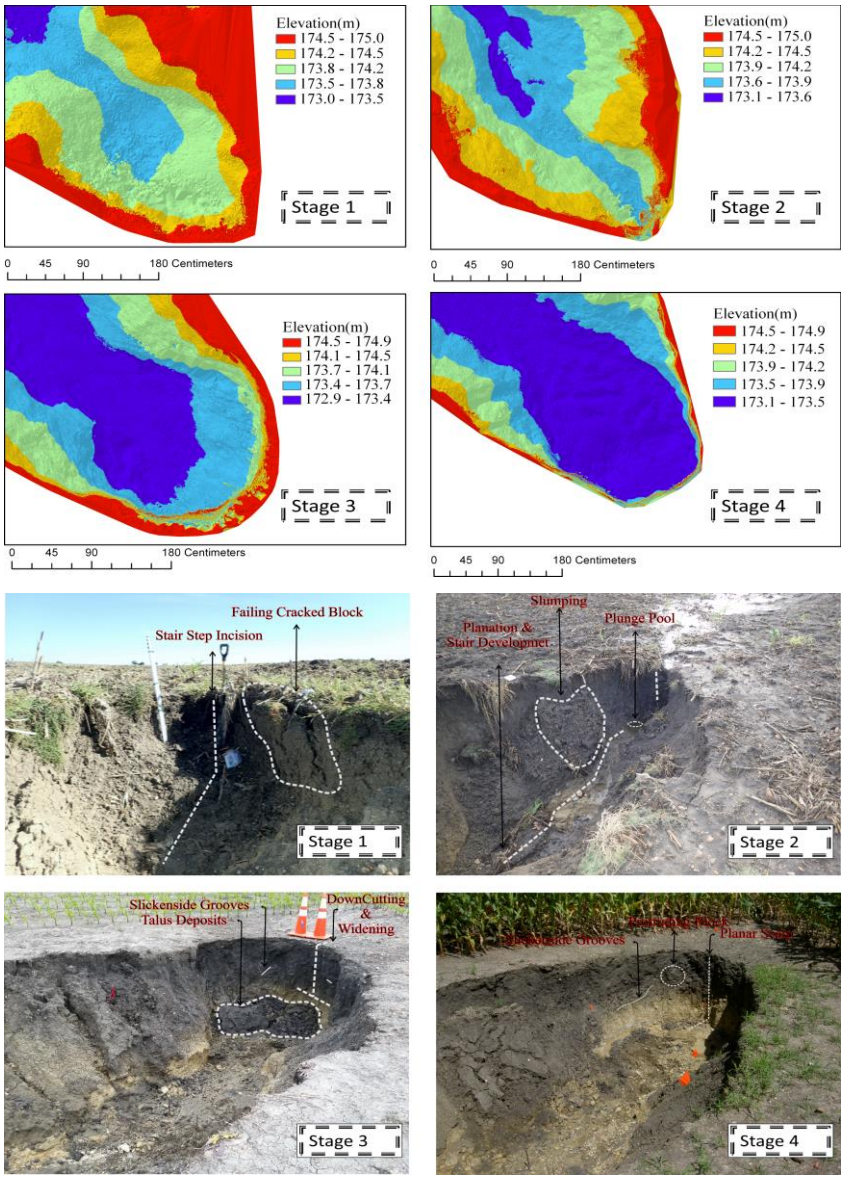

Figure 11: Growth stages of a permanent cohesive gully with a layered lithology. SFM DEMs and time-lapse images are shown. The growth stages illustrated are not all temporally sequential. Stages 1-2 and 3-4 occur sequentially. However, they all occurred within a 7-month period. Time lapse observations validate model structure

According to Collison (2001), headcuts go through cycles of instability due to pore water stresses as a result of preferential flow drainage through cracks and discharge. As stress is released, failure occurs either basally or along regions of high stress that have developed in fissured zones (Collison, 2001). Some field observations differentiate gullies within the study area. Tension, drying, and cracking leads to block and shear failures at the headcut scarp during storm events. Table 4 and Figure 9 showed that infiltration is an important consideration within these headcuts, while Figure 11 shows the development of tension cracks at the headcut during drying.

Based on Hanson et al., (2001), time-lapse videos, observations, reconnaissance, and structure-from-motion time-lapse models, the transitions occurring during the migration of a permanent Black-Land gully were documented. Figure 11 chronicled the probable evolution of the headcut in achieving stability, using structure-from-motion methods (1st phase). An accompanying reconstruction image is included at each stage for validation, with various morphologic features of the erosion process. During the growth stage descriptions, references are made to the delineated lithologic zones shown in Figure 3. Additionally, Table 8 documents the morphology of the headcut at each stage.

Table 8: Head-Cut morphometrics of gully growth stages. Average width ($\overline{W}$), depths ($\overline{D}$) and sideslopes (Left: $\overline{LSS}$ and Right: $\overline{RSS}$) were measured at the mouth center and brink of the head-cut. HC Height is the headcut height, while Bed-Hc Slope is the slope measured from the base of the scarp (HC Height) to the channel slope.

Stage	$\overline{W}$ (m)	$\overline{D}$ (m)	$\overline{WD}$ Ration (m)	Bed-Hc Slope (m m^{-1})	HC Height (m)	$\overline{LSS}$ (º)	$\overline{RSS}$ (º)
1	1.60	0.81	0.79	0.26	0.3	57	47
2	2.01	1.02	0.99	0.26	0.6	50	49
3	2.45	1.45	0.99	0.21	0.8	63	69
4	2.40	1.49	0.91	0.16	1.0	63	68

1.3.3.1 Stage 1: Initiation. During this stage, a series of stair-stepped headcut incisions occurred at the headcut. The incisions occurred along shrinkage crack locations where the cracks daylight to the gully face. The depth of the cracks is at the interface with the highly weathered shale zone about 1 m below the surface. During storm events, water flows down the crack until it hits a layer with more cohesion that is less easily degraded during the storm cycle. Over time, the upper meter is undercut and falls into the gully bottom to be entrained. The lower, more cohesive layer formed a 0.3-m bench above the gully bottom. Evidence of earth flows and scour were seen at these gully heads. Figure 11 (stage 1) depicts the primary gully head and shows that the top 20 cm of the soil profile retreated further than the lower soil zones. Failing cracked blocks were observed protruding from the upper soil horizon after drying. Table 8 shows that the headcut height was lowest at this stage, with steep side slopes. The width-depth ratio was at its minimum, and the slope from the base of the overfall was relatively consistent.

1.3.3.2 Stage 2: Planform incision. Stage 2 is characterized by an increase in the headcut height. As the upper zone recedes, the overfall lip has narrowed and flow width over the gully narrows; this increases flow and stream power to the gully bottom. The previous bench is eroded during this stage, and the bottom material is entrained. When the scarp height exceeds its critical height, the headcut becomes less stable. Figure 11 (stage 2) shows that vertical scour and side slope slumping increased. A plunge pool formed at the headcut base as the lower bench was eroded.

Plunge pools form within cohesive sediment when the stress applied by water flowing at the overfall is able to initiate scour at the soil surface. Several factors related to upstream and downstream conditions, the characteristics of the eroding bed material and

the erosive ability of water impact the development of plunge pools over time (Ploumis-Devick, 1985). Instability at the headcut occurs by the weakening of the base of the overfall; a factor observed to be effective for smaller upstream gradients and long-duration scouring times (>2.75 hrs.) (Ploumis-Devick, 1985). As such, it is possible to infer that the development of plunge pools is dependent on the erodibility of the actively eroding bench, discharge, and headcut height. According to Flores-Cervantes et al., (2006) discharge is mechanistically more influential to headcut retreat for plunge pools in diffusion, while scarp height is important in non-diffusive conditions. The latter describes the condition where the velocity of water at the bottom of plunge pools, and the water surface is similar; the former refers to a decrease in velocity as water approaches the plunge pool bottom. As such, overfalls in non-diffusive states may directly erode the soil surface.

Figure 11 (Stage 2) shows a plunge pool of at least 20 cm deep at the base of eroding bench where discharge ponded after the storm event. Plunge pools had two observed functions:

a) They acted like a pond for flow accumulation, which over time contributed to the weakening of the actively eroding soil zone.
b) They also increased moisture connectivity to the basal layers, evidenced as smaller hollows and pools at pockets along the incising plane.

1.3.3.3 Stage 3: Expansion. As the gully height increases ($> H_{critical}$), the side slopes are undercut and leads to slope failures on each side of the receding headcut. Over-fall discharge leads to erosion, block and shear type failures in conjunction with cantilever failures, with the corners of the scarp face failing along distinct planes. As sediment is entrained, the base of the headcut is more prone to undercutting by fluvial erosion. This

stage is marked by the start of a more linearly eroding vertical scarp as the downstream slope from the headcut is much flatter than previous stages. Figure 11 (stage3) shows a wider and more curvilinear morphology with increasing bed exposure as headcut height increased. Slickensides features were observed within the corners of the scarp at approximately 70º from the soil surface, shown in the image. Observations of the accumulation and dispersal of talus were indicative of this stage, compared to prior stages. Based on Table 8, the average width depth ratio was similar to stage 2. However, the bed to headcut slope gradient was shallower than the preceding stage. Side slopes were greatest at this stage (about 19º more than stage 2).

1.3.3.4 Stage 4: Stabilization. During stage 4, the headcut was at its greatest depth from $H_{critical}$; however, it was stable. The headcut height was within the range estimated by the USDA as the depth to the restrictive layer (1-1.7 m). The exposure of Taylor Marl was telling of this stage as downcutting was further constrained by Taylor sediment. Talus accretion was lowest, and sediment was typically entrained after failure. Lower soil zones were prone to fluvial undercutting as flow ponded at the headcut base and fanned out into base and banks. Figure 11 (Stage 4) shows a more planar scarp morphology in planform and front view, with a flattened channel bed. Table 8 shows that the average width, depth and side slopes of the headcut did not show a significant change. However, the bed to headcut slope was closest to the current channel slope of 0.11 m m^{-1}.

Crop growth was a distinguishing characteristic of this stage. Many knick-points and less developed gullies within the study area were associated with natural vegetation at the gully head. Studies have documented that the roots of plants impact slope stability (Osman & Barakbah, 2006) and cohesion (Ali & Osman, 2008). Vegetation increases the

shear strength of soils. Shear strength generally increases with increasing root density due to the additional tensile strength of roots. Additionally, increases in erosion resistance are spatial and temporal, with surficial soil layers showing the greatest contribution to cohesion. Shear strength attributed to roots was shown to vary from 26 to 183 kPa by Osman & Barakbah (2006), while cohesion varied up to 34 kPa by Ali & Osman (2008) for different vegetation types. The shear strength of soils with roots may be up to 100 percent greater than without roots (Fan & Su, 2008). Soil cohesion near the bank top was estimated in excess of 200kPa within the study area (Allen et al. 2017). Migration at this stage occurred more slowly and linearly along the vertical scarp profile, although undercutting sometimes created minor overhangs during retreat.

1.4 Discussion of Results

1.4.1 Migration Factors

Variations in the magnitude, frequency, and duration of rainfall events, in conjunction with drought periods, have been associated with the formation and cutting of gullies within the semi-arid regions of North America (Bull, 1997). Long-term precipitation evaluations by Harmel et al., (2003) shows that on average 11 days per year have rainfall greater than 25 mm within the Black-Land Prairies. For the study period, 18 days had rainfall greater than 25 mm, with 6 days greater than 50 mm. Work by Harmel et al., (2006), has shown that rainfall contributes to significant variability in runoff volumes and peak flow rates within Black-Land agricultural catchments. Moreover, runoff and flow rate changes within catchments impact the seasonal loss of soil (Harmel et al., 2006). As such, understanding the factors that might be most influential to retreating headscarps due

to changing or increased convective activity might be influential to future modeling attempts within the region.

To identify the parameters most influential to a retreating Black-Land gully, bivariate correlation analyses were done. Table 9 summarizes these relationships and their significance levels within a correlation matrix. The red box highlights the section of the matrix discussed further. However, the factors impacting migration were interdependent. More than one factor may simultaneously impact retreat and soil water conditions. Table 9 also agrees with Harmel et al. (2006), showing strong correlations between rainfall factors and discharge within the study area.

Table 9: Parameter correlations informing head-cut migration. Soil moisture related factors are Antecedent API (soil moisture from the last migration event), Peak API (maximum moisture during rainfall events) and Pre-API (moisture when migration was measured)

		Precipitation	Average Intensity	Events > 10mm	Dry Days	Peak Discharge	Antecedent API	Peak API	Pre API
Precipitation	Pearson Correlation	1	.880**	.844**	.921**	.898*	0.483	.896**	-0.224
	Sig. (2-tailed)		0.004	0.008	0.001	0.015	0.226	0.003	0.593
	N	8	8	8	8	6	8	8	8
Average Intensity	Pearson Correlation	.880**	1	.758*	0.677	.853*	0.112	.871**	-0.019
	Sig. (2-tailed)	0.004		0.029	0.065	0.031	0.792	0.005	0.965
	N	8	8	8	8	6	8	8	8
Events > 10mm	Pearson Correlation	.844**	.758*	1	0.636	.831*	0.529	.924**	0.267
	Sig. (2-tailed)	0.008	0.029		0.090	0.041	0.177	0.001	0.523
	N	8	8	8	8	6	8	8	8
Dry Days	Pearson Correlation	.921**	0.677	0.636	1	0.406	0.557	0.688	-0.550
	Sig. (2-tailed)	0.001	0.065	0.090		0.425	0.152	0.059	0.158
	N	8	8	8	8	6	8	8	8
Peak Discharge	Pearson Correlation	.898*	.853*	.831*	0.406	1	0.113	.927**	0.810
	Sig. (2-tailed)	0.015	0.031	0.041	0.425		0.831	0.008	0.051
	N	6	6	6	6	6	6	6	6
Antecedent API	Pearson Correlation	0.483	0.112	0.529	0.557	0.113	1	0.522	-0.037
	Sig. (2-tailed)	0.226	0.792	0.177	0.152	0.831		0.184	0.931
	N	8	8	8	8	6	8	8	8
Peak API	Pearson Correlation	.896**	.871**	.924**	0.688	.927**	0.522	1	0.184
	Sig. (2-tailed)	0.003	0.005	0.001	0.059	0.008	0.184		0.662
	N	8	8	8	8	6	8	8	8
Pre API	Pearson Correlation	-0.224	-0.019	0.267	-0.550	0.810	-0.037	0.184	1
	Sig. (2-tailed)	0.593	0.965	0.523	0.158	0.051	0.931	0.662	
	N	8	8	8	8	6	8	8	8
Migration	Pearson Correlation	.952**	.740*	.728*	.979**	.907*	0.554	.775*	-0.443
	Sig. (2-tailed)	0.000	0.036	0.041	0.000	0.012	0.154	0.024	0.271
	N	8	8	8	8	6	8	8	8

**. Correlation is significant at the 0.01 level (2-tailed).
*. Correlation is significant at the 0.05 level (2-tailed).

1.4.2 Precipitation Factors

Precipitation is the most important agent for erosion. In a global study by Vanmaercke et al., (2016), the rainy day normal was shown to be the most important variable explaining the volumetric retreat of gullies. However, the impact of rainfall during erosion depends on rainfall characteristics such as the storm intensity, duration, frequency, number of events, and drying. Rainfall leads to erosion through reductions in shear strength, soil detachment or changes in matric potential at the soil surface as raindrops impact the ground (Cruse & Larson, 1977). A study by Osborn & Simanton (1986) suggested that the number of rainfall events had a greater impact on migration than the magnitude of the event. Additionally, Rieke-Zapp & Nichols (2011) showed that events exceeding a particular intensity threshold were significant predictors of retreat. Ultimately, high-intensity showers may lead to inter-rill and rill erosion when the applied shear stress of raindrops exceeds a detachment threshold.

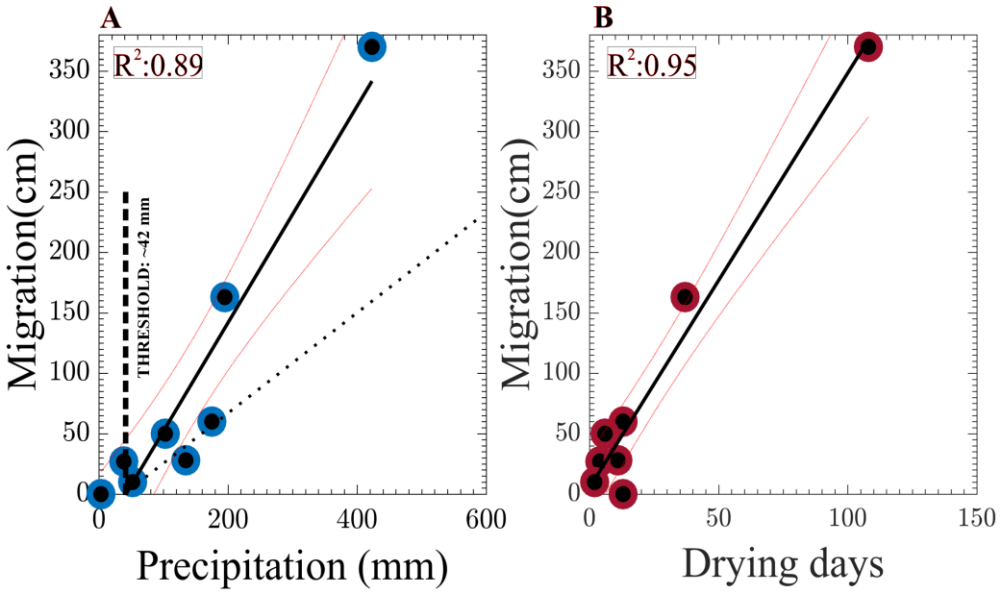

Figure 12: Linear relationships of the factors most strongly related to the headcut migration of tributary 1. A: cumulative rainfall between retreat periods, B: Drying days between periods

Rainfall characteristics showed moderate to strong correlations with migration (Table 9). Figure 12 displays the strongest factors influencing retreat. An R^2 of 0.89 and 0.95 were determined for precipitation totals and drying days between events, respectively. Red lines show the 95% confidence interval. Each point within the dataset represents individual time-steps or events where retreat was measured.

The periods of greatest retreat in Figure 12A coincide with greater drying days in Figure 12B. Moreover, migration generally increased as rainfall totals and drying days increased. As such, greater rainfall totals with protracted drying days increase headcut migration. To illustrate such an example: Figure 12A shows a greater change in retreat for data points above 175 mm of rainfall, shown as the difference between the fitted data and dotted line. Comparing the 175-mm and the ensuing 195-mm rainfall event, with 3 times more drying days for the latter event, retreat was 2.7 times greater. This association can explain much of the scatter in the data set.

The greater impact of drying days is related to Vertisol cracking, which is associated with the breakdown of soil microstructure and increased infiltration (Kishné et al., 2010; Arnold et al., 2005). Based on Figure 9 and Table 4, infiltration increased after dry periods, with the effect being greater during the growing season (period 2). The cropping period spanned from mid-May to July. The increase in infiltration was thought to be related to the opening of cracks during the dry soil water phase, which increases soil cracking (Arnold et al., 2005b) (Figure 4). Cracks generally form within soils that show shrinkage and swelling properties; this is related to changes in volume that occur as moisture changes within the soil profile. Additionally, the growth of roots within the soil profile during plant maturation may contribute to increased infiltration, decreased surface

runoff, and the drying of soils, as plant available water is used. Hence, shear strength may decrease due to infiltration and pore pressures changes (Collison, 2001).

The influence of rainfall intensity and the number of rainfall events between migration periods were assessed using observed rainfall data for the events in Figure 12. The comparison was made using the average intensity for individual storms between migration periods, based on the same number of storms used for evaluations of the effect of number-of-rainfall events between migration periods. Rainfall intensity and number-of-events explained 47% and 45% of the variability in the precipitation-migration relationship. Given that rainfall totals between migration periods accounted for 89% of the variability in migration as in Figure 12A, rainfall intensity and number-of-events showed no comparatively greater significance within this factor. Each accounted for ~50% of the effect of total rainfall between periods. Based on Table 9, the effect of intensity and the number of events were more closely related to soil moisture and discharge.

The x-intercept of Figure 12A (42 mm) was interpreted as a precipitation threshold, defined as an estimate of the rainfall total promoting headcut migration for gullies within the study area. All points in Figure 12A were greater than the estimated threshold, except at the origin where no migration occurred. However, it is recognized that migration may also occur due to the cumulative effect rainfall on soil moisture conditions between periods. Changes in soil moisture impact soil susceptibility to erosion.

1.4.3 Moisture and Strength Relationships

Soil erodibility is related to percent clay, clay type, and soil density (Hanson et al., 2010). Work by Henderson et al., (2006) has shown that erodibility is also influenced by antecedent processes such as wetting and drying, and freeze-thaw cycles. Prewetting or

high moisture contents make soils more susceptible to erosion by rainfall (Wolman, 1959). This is associated with a decrease in the strength of interparticle forces within soil. However, drying of Vertisols causes cracking as soils rich in smectite clays shrink with seasonal water deficits, which are influenced by soil evapotranspiration. Within the Black-Land prairies, Arnold et al., (2005) has shown that evapotranspiration (ET) shows a similar temporal trend to the development of cracks (Figure 4). An approximate three-month lag between cracking and ET was observed. However, as soil moisture decreases, tension forces develop within the soil matrix that eventually force water out of contact sites within soil (Kemper et al., 1987). At lower water contents, soil shear strength increases (Kemper & Rosenau, 1984). However, drier soils mean more cracking, which weakens soil and increases its susceptibility to entrainment (Couper, 2003).

As stated, clay content and bulk density impact the strength of cohesive soils. Higher clay contents are associated with greater critical shear stresses and a lower potential for inter-rill erosion (Line & Meyer, 1989; Gilley et al., 1993). According to Robinson & Hanson, (1995b), increases in material density are associated with greater unconfined compressive strength and lower retreat within headcuts. The increase in strength is related to greater numbers of interparticle contacts between soil grains promoting cohesion (Mitchell, 1964). However, individual factors impacting erosion may show poor predictive ability since many factors may simultaneously influence erosion. This codependence has been reviewed by Knapen et al., (2007). Works by Sheridan et al., (2000) and Allen et al., (1999) have showed improved correlations when multiple factors impacting erodibility have been simultaneously evaluated.

Relationships between soil moisture and shear strength were used to evaluate the conditions promoting retreat. The peak API was used for evaluations; of the moisture-related factors, it was most strongly correlated with retreat (Table 9). Peak API represents the maximum soil moisture between migration events. Figure 13A shows this relationship with an R^2 of 0.6 and an API intercept of 65 mm. Red lines show the 95% confidence interval for the data set. All points fall within or at the confidence limits. The intercept was interpreted as a wetness threshold for retreat. Based on Figure 7, the average API during the monitoring period was 63 mm. Therefore, soil moisture was on average slightly below the wetness threshold for retreat to occur, and was therefore susceptible to erosion and weakening by moisture increase. Using the API-moisture regression from Figure 8, the threshold moisture condition was estimated at 34% (Field capacity) ± 5%, the variability representing the potential uncertainty in moisture evaluations by (3).

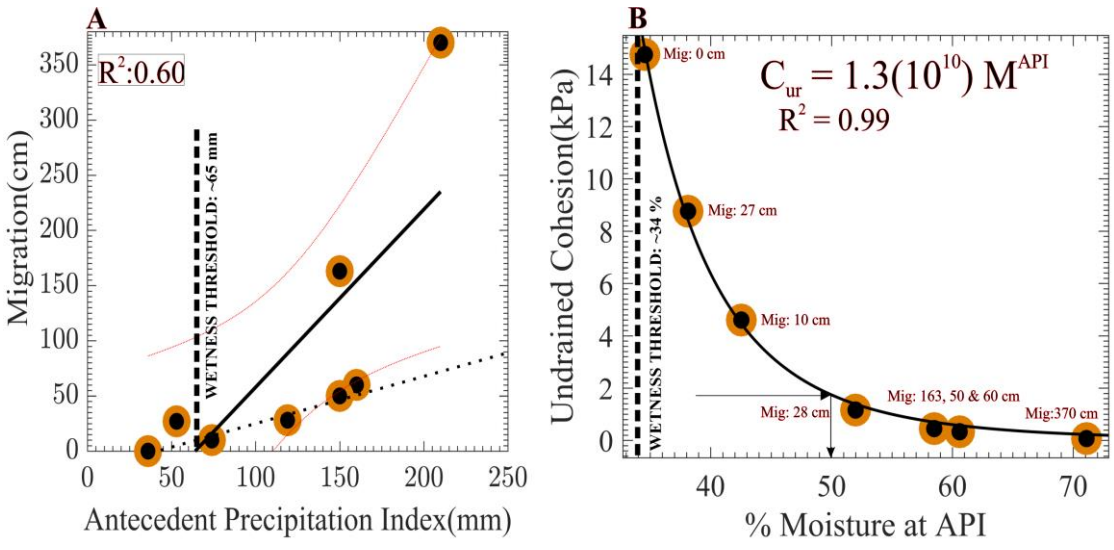

Figure 13: Moisture strength relationships during headcut retreat (A) Relationship between Peak API and migration (B) Moisture-cohesion relationship based on API by (5)

$$C_u = C_L 35^{(1-I_L)} \quad (5)$$

where C_u is the undrained cohesion, C_L = 1.7kPa and 0.2< I_L<1.1 is the liquidity index defined as $\frac{W_c\text{-}PL}{LL\text{-}PL}$; W_c is water content, PL is the plastic limit, and LL is the liquid limit

$$C_{ur}=1.3\left(10^{10}\right)M_{API}^{-5.8} \quad (6)$$

where C_{ur} is the undrained cohesion during retreat, and M_{API} is the moisture content based on API

RHS constants vary between (-1.0×10^{10}): (3.7×10^{10}), and (-6.3): (-5.3) at the 95% confidence interval

The shear strength of soil at the wetness threshold was interpreted using (5), derived by Vardanega & Haigh (2014) which estimates undrained cohesion with volumetric water content based on extensive studies of clay soils. Equation 5 is based on the liquidity index (I_L) which is the ratio of moisture at the geotechnical limits of soil. According to Vardanega & Haigh (2014), I_L may vary increasingly for values greater than the equation boundaries. As such, the limits of (5) were strictly conformed to. Using the regression of API and soil moisture (3), peak API for each migration event shown in Figure 13A was converted to percent moisture. Then, undrained cohesion for each event was estimated based on the predicted soil moisture using (5), shown in Figure 13B. The figure shows the relationship between percent moisture and cohesion for each event using a first order power function as (6). (6) was estimated with an R^2 of 0.99, and an RMSE of 0.26. Each value within the figure is labeled with the retreat occurring for the moisture-undrained cohesion condition. The figure shows that headcut retreat generally occurred at or above field capacity, although one point within the dataset was slightly lower. The difference was not significant, varying from the API threshold by about 10 mm, and falling within the variability for moisture evaluations. Figure 13B shows that the shear strength at the wetness threshold

was approximately 14KPa. Therefore, migration occurred when undrained cohesion was less than 14kPa, i.e., the undrained cohesion related to the wetness threshold.

Figure 13B shows that retreat increased as shear strength decreased, with increasing moisture. However, changes in this trend were related to differences in growing conditions and precipitation characteristics. Solid vertical and horizontal arrows are used to highlight a region of discussion in the dataset with estimated soil water contents greater than 50%, and undrained cohesion less than 2kPa. Data points with the lowest migration values (28 and 50-cm) occurred under growing conditions. Further, the 163, and 60-cm migration events occurred under the same growing conditions, but also represent the difference between the fitted and dotted lines shown in Figure 12A, already discussed. Vegetation may contribute to decreases in gully growth during high moisture conditions by increasing soil cohesion. Consequently, the decrease in undrained cohesion was regarded as a preparative influence on headcut retreat since different retreat magnitudes may occur under similar moisture conditions.

The relationships between cohesion and retreat shown as Figure 13B was marked by two notable uncertainties. The API-migration relationship varied with land use, as stated. Regression coefficients of 0.64 and 0.94 were estimated during the uncultivated and cropping periods respectively. Two show this difference within the dataset, a dotted line was used to represent a fit of the points occurring under vegetation conditions in Figure 13A. The fact that peak API was a better predictor during cropping suggests that higher moisture contents may have a greater impact on migration during crop growth. During the uncultivated period, more rapid fluctuations in retreat occurred, attributed to variable discharge and drying. Additionally, soil moisture was prone to rapid changes due to rainfall

intensity per event. High-intensity storms were related to smaller increases in moisture and higher runoff. As such, the shear strength relationship may be more applicable for low-intensity storms. Moreover, the dominant failure mechanism of the headcut may change based on this interchange between the influence of high runoff and greater moisture responses. The soil moisture response to variable intensity agrees with findings by Hottenstein et al., (2015) for rainfall under messic climatic regimes.

1.4.4 Vertical Changes In Moisture Within Soil Zones

The evolution of the gully scarp was related to vertical changes in moisture (Figure 14). Here the changes in moisture with rainfall at the top (0.1 m), middle (0.4 m) and base (1.1 m) of the headcut are shown in 10-minute time increments for about 50 hours, contiguous with the initial storm phase of period 3 (Figure 8). Measurements were made along the soil surface of the headscarp. Two images to the right of the figure are of dried and moist scarp conditions. The dried scarp highlights cracks along the gully face, shown as white lines.

Moisture varied significantly with depth from the soil surface. Within loess gullies, Van Den Elsen et al., (2003) showed the soil surface layer has greater moisture variability than lower layers. Figure 14 shows a similar trend. However, differences of 12% and 30% were initially measured along the scarp with increasing depth. Deeper soil zones showed a greater volumetric moisture and delayed or negligible moisture responses. At the headcut base (Zone 3), water content was initially more than three times higher than the top, despite coinciding with the driest period.

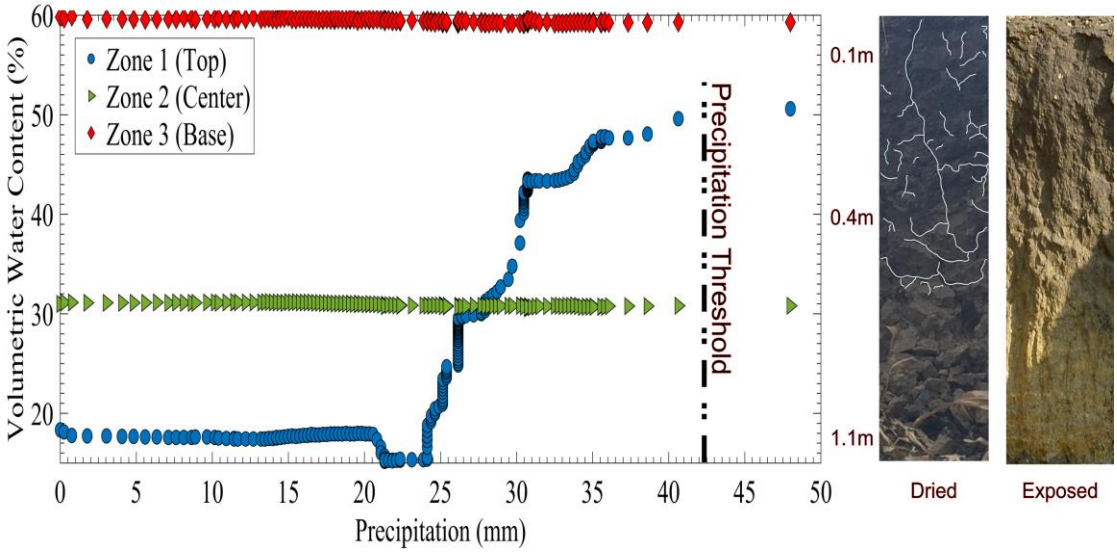

Figure 14: Vertical variability in soil moisture with increasing rainfall. The Erosion threshold predicted by Figure 12A is displayed. The event recorded was part of a 174 mm rainfall event which resulting in the morphology in Figure 9B.

Soil moisture within the top 0.1 m (Zone I) was susceptible to rapid fluctuations, increasing during wet periods and undergoing rapid decay during dry periods. Figure 14 shows that soil moisture was initially between the wilting point (16%), based on Saxton & Rawls (2006) and the plastic limit (20%). Soils with a greater range of volumetric water contents where plastic behavior occurs, i.e., having greater plasticity indices, are more susceptible to shrink-swell behavior, and have greater water holding capacity (Puppala et al., 2013). As such, the lower plasticity of Zone I suggests that the soil zone may gain and lose strength faster rate than lower soil horizons. After 24 mm of rain, moisture started to increase. Abrupt changes in water content ensued. By summing up the 10-minutes time increments for moisture measurements on an hourly time-step, the maximum change was 8%. These changes were attributed to variable infiltration through cracks, and partly explains the variability in runoff occurring within these soils. During moisture increase, field capacity and saturation were exceeded. After 40-48 mm of rain, the soil reached its

liquid limit of 53%, which according to Vardanega & Haigh (2014) may represent a fixed strength where soil starts to flow. Based on 5)4, these evaluations of soil moisture indicate that soil cohesion varies vertically within the receding headcut.

Because the liquid limit is associated with loss of shear strength, the point at which it is reached in the soil profile should be indicative of the moment at which the soil begins to fail in the headcut. The total rainfall required to reach the liquid limit (40-48 mm) was similar to the predicted precipitation threshold (42mm) for retreat to occur (Figure 12A). Within the precipitation range where soil liquidity was reached, soil moisture readings decreased, a factor attributed to the loss of contact between moisture probes and the headcut surface as the soil became more fluid. Because of the agreement between these precipitation totals assessed using two different procedures, it stands to reason that the loss of strength at the liquid limit is an important point in the retreat of headscarps. Although migration may occur under various conditions, the liquid limit might be an equally important soil property governing retreat. This stands to agree with Vanmaercke et al. (2016)'s claim of the importance of soil cohesion

1.4.4.1 Impact of moisture changes within soil zones. The vertical variability in soil moisture influences the headcut growth stage during retreat. Figure 15A depicts the post-event morphology for the moisture evaluation in Figure 14. The top, transition, and base of the headcut retreated at different rates by a stair-step failure mechanism. Lower clay content, lower bulk density, and lower plasticity index of soil near the headcut surface made the headcut top the most erodible region. This evaluation agrees with erodibility estimates from Table 1 with depth from the soil surface.

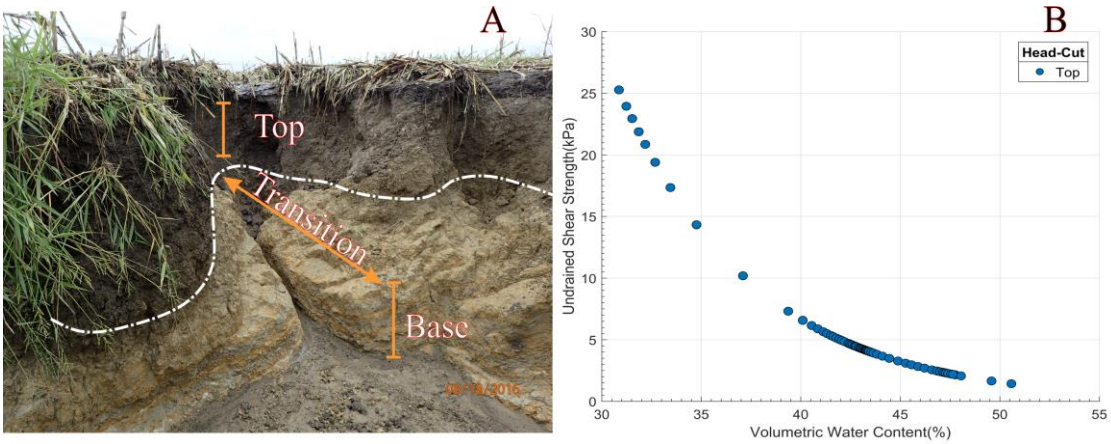

Figure 15: Differential soil zone failure. A: Post event morphology after a total of 174 mm of rain over 6 days, which includes Figure 9 .B: Undrained cohesion-moisture relationship at 0.1 m depth based on (Figure 9) by (5).

The erosive factors impacting retreat were low shear strengths (Figure 15B), high runoff and infiltration (Figure 9), and longer drying days (Figure 8). Figure 15 shows that the vertical gradient in soil moisture contributed to vertical changes in unconfined cohesion. The top of the headcut was below its plastic limit prior to the storm. As moisture increased, soil shear strength showed steady hyperbolic decrease until about 40% moisture, after which shear strength was minimal. The middle and base of the headcut showed positive liquidity indices before and during the moisture assessments with the base being closer to its liquid limit. Therefore, the rate at which moisture and strength changes at these topographic positions or soil zones influences retreat and the headcut morphology.

Changes in moisture also influenced failure at regions near the bank of the headcut. For day 1085 (period 1) (Figure 8), evidence of soil loss was observed as bank slides. Sliding created localized scour regions, prone to failure during successive storms. Scoured banks were observed as changes in the geometry of bank microfeatures and incision along preferential flow paths. However, during other storms within the same period, a tandem of infinite failures and slides were observed from storm videos, which altered the morphology

of the headcut and banks simultaneously. The latter was associated with higher rainfall intensities, greater runoff, and comparatively lower moisture measurements.

1.4.5 Runoff and Migration

Headcut migration was driven by runoff and discharge at the gully head. Migration trends generally followed changes in runoff occurring during the simulated periods (Figure 9). Table 9 shows that discharge was most strongly related to moisture conditions via peak API, having a correlation coefficient of 0.93. Greater discharge was associated with higher moisture conditions. Runoff occurs either from high-intensity storms that exceed the rate at which rain can infiltrate soil or through a gradual increase in soil moisture. As moisture increases within a soil profile, pores within the soil matrix are filled up to saturation. As saturation is exceeded, runoff occurs. While moisture conditions were regarded as subaerial influences which decreased the strength of soil, the effect of discharge at the overfall was the driving force for scarp retreat.

Rainfall events producing greater discharge increased headcut retreat. Moreover, differences in discharge best explain the increase in migration of tributary 2 during short-term evaluations. An ephemeral channel connecting gullies 2A and B (Figure 1) developed and became increasingly incised during monitoring. The developing gully provided a pathway for funneling runoff from catchment 2B into 2A. Figure 16 shows that peak discharge may account for 78% of the variability in retreat ($R^2 \approx 0.78$). The red lines in the figure show the 95% confidence interval. Peak discharge was assessed as the maximum discharge occurring for each migration period. This differs from the work of Robinson &

Hanson (1995a) who found no statistically significant increases in advance rate with discharge during continuous discharge experiments at similar overfall heights. However, the study was conducted for storm discharges between 0.5 $m^3 s^{-1}$and 2.5 $m^3 s^{-1}$. According to Robinson & Hanson (1995a), retreat due to water flowing at a headcut may be impacted by aeration, defined as the development of an air pocket beneath flowing water at an overfall. Increased aeration leads to lower stresses at the base of the overfall because water impacts the channel bottom a greater distance from the scarp face. Due to the low catchment gradient and lower discharge, the gully head was largely in a non-aerated state. As such, the strong correlation in Figure 16 might be attributed to greater stresses at the headcut base.

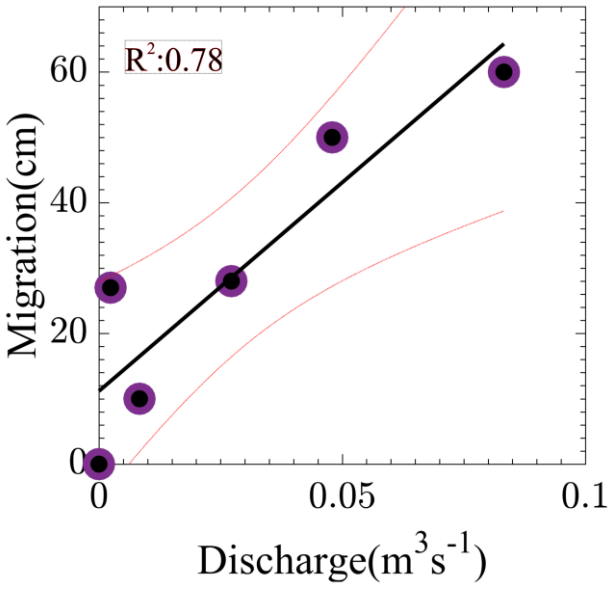

Figure 16: Relationship between peak discharge and headcut retreat.

$$\frac{\Omega_s}{\Omega} = \frac{\rho_s Q_s}{\rho_w Q_r} \tag{7}$$

where ρ is the sediment (ρ_s) and water densities (ρ_w), while Q refers to sediment discharge (Q_s) and runoff (Q_r) discharges.

The growth of crops decreased soil loss by a factor of 3 during cultivation (period 2). To quantify this effect, an erosion efficiency metric based on Thomas et al. (2004) was used. Erosion efficiency refers to the ratio of stream power required to entrain sediment, defined by (7). Runoff discharge was estimated as the average peak discharge using the

staff gauge and rating curves, while sediment discharge was assessed from SFM-volumetrics. To normalize the data set, all calculations were done on a daily interval. An approximate three-fold decrease in the efficiency ratio (0.003:0.0009) was estimated as crops matured, which agrees with the impact of crops described in Figure 13. A larger efficiency ratio number implied that there was more sediment being lost at the headcut for a particular discharge. In other words, less sediment was lost as crops matured. This finding is analogous to results by Pathak et al., (2013) on Vertisols in India. The average sediment concentration under maize and sorghum intercrops decreased by approximately half during the growing season.

1.4.6 Multiple Linear Migration Factors

$$\mathrm{HC_{Migration}} = 0.312(\mathrm{Precip}) + 2.363(\mathrm{Dry\ Days}) - 12.6 \quad (8)$$

where $\mathrm{HC_{Migration}}$ is the headcut retreat in cm; Precip is rainfall in mm; Dry Days is drying days

Several factors influenced headcut migration (Table 9). Multiple linear regression analyses of these factors are shown in Figure 17. The regression of precipitation and drying days outperformed all other factors, shown as (8). An adjusted R^2 of 0.97 and standard error of 22.9 was estimated. The regression equation indicates that drying days has a stronger effect on $\mathrm{HC_{Migration}}$ than precipitation.

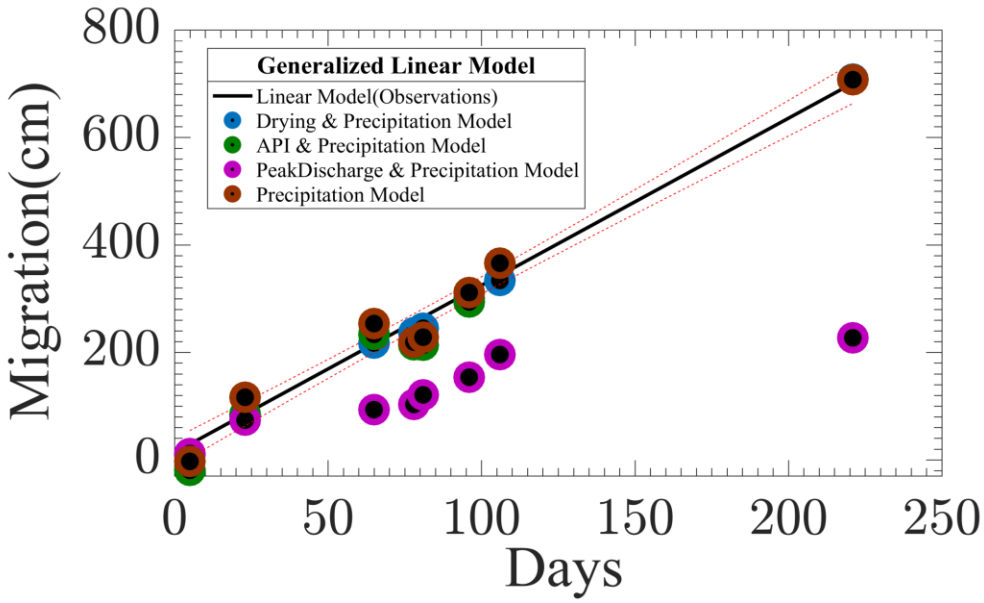

Figure 17: Multiple linear regressions of parameters with the strongest correlations.

Drying of soils is a critical factor impacting the susceptibility of soil to erosion. According to Hottenstein et al., (2015), cumulative drying days and soil moisture differentially affect the moisture response of regions with average rainfall less than 500 mm (semi-arid) and rainfall greater than 500 mm (messic). Cumulative drying days was a more significant factor for regions within semi-arid climates on an annual timescale. In this study, observations suggest that drying days is still a significant factor influencing soil moisture and the susceptibility of the gully head to erosion on an event basis, despite the messic climatic regime. Drying days was regarded as a factor related to subaerial conditions, particularly influenced by solar irradiation and the shrink-swell potential of soils.

Solar radiation influences the rate at which different regions of the gully dried. Time-lapse videos show that the right bank was more exposed to sunlight than the left. This was related to the relationship between the solar illumination angle and bank azimuth.

To quantify this effect, the shade 2 model (Li et al., 2012) was used to express the time of exposure for both banks of the channel using estimates of the effective shadow length. During model simulation, the total exposure time was assessed based on the simulated time when the bank shadow length exceeded the average channel width of the region above the camera point of view.

Figure 18A shows the simulated exposure times for both banks, while Figure 18B is used to verify model accuracy from time-lapse images. Four days were chosen to demonstrate the variability in bank exposure, choosing days within each of the soil water phases of the Black-Land Prairies, as described. Exposure was greatest during the saturated and dry phases. The figure shows that the right bank was exposed to greater sunlight. However, the right bank exposure time was less later in the year (Sept, Dec). This is related to the solar analemma because the position of the sun in the sky varies as observed from a fixed position as the year progresses. A comparison of moisture readings at the banks revealed that the left bank was susceptible to a more rapid decline in moisture content. To determine model uncertainty, percentage shade was estimated on a day with clear skies and no vegetation. Clouds and vegetation may cast shadows in the gully and act as an additional source of uncertainty. A series of grids were graphed over the image, and the percentage of shaded grids were estimated by counting. Figure 18B illustrates the counting grids used. The shaded bank accounted for 39% of the total image. The simulated exposure was 28%. As such, a difference of 11 percent as estimated under ideal atmospheric conditions (clear skies, no vegetation) may give an indicator of the potential variability in exposure times depicted in Figure 18A

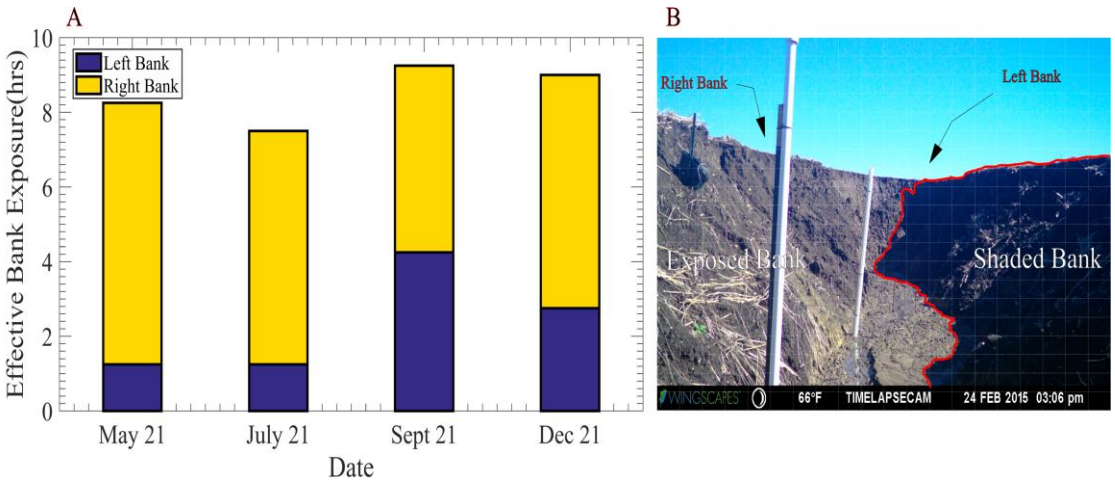

Figure 18: Impact of solar azimuth on bank exposure to solar irradiation during drying based on Li et al. 2012 (A) Variable exposure of gully banks on a daily cycle. (B) Image of gully bank used for model verification

The shrink-swell potential of soil is an extensively studied soil property related to drying and cracking, typically assessed using the coefficient of linear extensibility (COLE) (Arnold et al., 2005a; Lepore et al., 2009). COLE is derived from laboratory assessments of soil shrinkage properties. It expresses the change in length of the soil matrix between field capacity and when it is dried in an oven (Dinka et al., 2013). The API-soil moisture relationship in Figure 8 simulates the development of cracks at APIs less than 50 mm. As such, cracking was most influential to retreat during period 3. Speculatively, drying days may prove an important proxy in the field, or in conjunction with COLE, help improve the predictive ability of gully models.

1.4.7 Comparison to other Cohesive Gullies

Few studies have related the material properties of soils and gully evolution at the field scale. Flume studies have traditionally been used because the factors influencing retreat can be more readily controlled. SFM and time-lapse imagery provided an avenue for high-resolution morphometric evaluations. Comparing the role of lithology in gully

studies conducted in Vertisols proved difficult because of inadequate reporting. The geotechnical properties of soils were unreported or not distinguished.

A few processes occurring at the gully head were comparable to other flume studies. Plunge pool erosion and undercutting impact the stability of cohesive headcuts. According to Ploumis-Devick, (1985), plunge pools increase the height of gully walls and induce instability. An increase in the height of the headcut was found to reduce the factor of safety. However, the effect was found to be greater when gully walls are undermined and for low catchment gradients. Similarly within this study, cantilever type failures and plunge pools were significant retreat mechanisms during the evolution of the headcut, as observed through time-lapse videos. However, failure by plunge pool erosion is believed to be more frequent in stages I and II, while cantilever failures occur prevalently in stages III and IV of the layered evolution model (Figure 11). Cantilever-type failures were observed as water flowed along the corners of the scarp. Additionally, impingement by water flowing at the over-fall is non-aerated because of low catchment slopes. This promotes vertical scour and planform-incision (Figure 11: Stage 2). Undercutting of the scarp was related to an increase in the backwater water level to the headcut ratio, and more turbulent flow at the headcut base. According to Robinson & Hanson (1996), increases in the backwater to headcut ratio promote greater redistribution of stress at the headcut base. This generally lead to a planar scarp geometry, shown as part of the transition from stages 3 to 4 in Figure 11. In Bennett et al., (2000), the removal of surface seals and the scouring of the bed by flow at the brink (Jet scouring) were significant factors in the development of headcuts. Surface seals refer to a protective soil layer or crust formed by disaggregated soil particles as a result of raindrop impact. These seals mitigate erosion and infiltration.

While scouring is significant for gullies with vertical scarps, infiltration contributed to failure within these gullies. Water infiltrating through cracks and the loss of strength at each soil zone due to soil-moisture increases contributed to the evolution of the stair-step morphology of the headcut and the failing of surface seals. As surface seals fail, the shear stress of concentrated overland flow more easily erodes Zone 1 (Figure 3), and leads to rill formation and incisions at the headcut brink. Subsequently, as water infiltrates through cracks, increases in pore pressures may contribute to failure (Collison, 2001). Under drying conditions, cracks formed at the face of the headcut within the Zone 1 as was shown in Figure 6: Stage 1, only to fail during subsequent storms.

Field-scale studies have tended to focus on migration rates and soil loss. However, a few factors influencing the formation cohesive headcuts have been identified. Groundwater table fluctuations and soil piping were identified by Frankl et al., (2012) and Zegeye et al., (2016) as significant contributors to gully development. Piping and subsurface erosion appear to be dominant features within gullies in Nigeria, while increases in moisture and groundwater table fluctuations have been identified as significant factors impacting gully development in Ethiopia. In soils rich in smectite clays, shrink-swell contributes to the formation of pipes by providing pathways for subsurface erosion. Where water tables increase, failure occurs by sliding of gully walls and slumping as lower soil horizons become saturated (Tebebu et al., 2010). For failures attributed to rising water tables, the gullies were associated with adjacent streams. At the study area, no evidence of piping or water table fluctuations were observed. However, the base of the scarp retained more water, largely attributed to the higher liquid limit. Gully initiation and migration along stream corridors were related to stream degradation, bank instability and runoff from

adjacent highways. The collapse of sediment along stream banks instigates incision into the failed bank material of lower strength. The effect is exacerbated by agricultural terracing, which concentrates runoff into lower lying regions of farm fields.

Cohesive gullies occur in regions of varying relief. In regions of high relief, the drainage area-slope threshold is informative as an initiation mechanism. High-relief or hill-slope related cohesive gullies can be found in China (Ding et al., 2017; Dong et al., 2014; Dong et al., 2013). However, subaerial processes are thought to have a greater impact in low-relief regions or where gullies form along stream corridors, as was the case in this study. Ding et al., (2017) showed that measurements related to profile lengths such as slope and elevation were significant factors related to the morphology of the gully. Work by Dong et al., (2014) showed that slope was an important factor related to the distribution of vegetation at the gully head, while vegetation distinguished active from inactive gullies. Within this investigation, slope was less germane to the migration of established gullies within catchments, while vegetation appeared to be important in decreasing gully erosion. The slower retreat of tributary 3 was attributed to increased channel vegetation. The importance of gradient was related to the initiation stage (Figure 11:stage 1) where rills formed within oversteepened regions around grasses, which Meyer et al., (1975) suggest is a factor not only related to slope but rather a threshold phenomenon impacted by concomitant factors such as soil type.

1.5 Conclusion

The development of gullies within the Black-Land Prairies was related to a rich history of agriculture and stream degradation. Changes in rainfall characteristics impacted the susceptibility of the gully head to migration. Of the rainfall factors assessed, the total

rainfall between migration periods showed the best predictive ability ($R^2 \approx 0.89$) Approximately, forty-two mm of rainfall was estimated for head headcut migration using linear regression analyses. However, the effect of rainfall was related to subaerial soil conditions. Subaerial conditions were regarded as preparative factors impacting the susceptibility of the gully head to migration during rainfall events, related to drying days ($R^2 \approx 0.95$), volumetric water content above a wetness threshold ($R^2 \approx 0.6$), and variable exposure to sunlight. Shear strength was an associated soil property further related to soil moisture ($R^2 \approx 0.99$) influencing headcut failure, particularly at the liquid limit. While shear strength was indicative of the susceptibility of the gully head to erosion, discharge was the driving force for retreat ($R^2 \approx 0.78$). These soils were susceptible to high surface runoff during wet periods, and high infiltration due to crack flow during dry periods; both related to the failing of the gully scarp. Overbank and channel vegetation were significant deterrents to headcut retreat, contributing to a decrease in erosion efficiency by a factor of three.

A distinct vertical zonation of the scarp was found to contribute to a layered evolution of the headcut, constrained by a less permeable shale unit. Four transient stages were identified using structure-from-motion, and time-lapse observations: Initiation, Planform-Incision, Expansion, and Stabilization. Structure-from-motion and the methodology used for gully monitoring proved useful in quantifying the changes occurring at the gully head, allowing for evaluations that were traditionally conducted in flumes to be translated into field practice.

BIBLIOGRAPHY

(NRCS) Natural Resources Conservation Service, 2017. Web Soil Survey. United States Department of Agriculture.

(USDA) United States Department of Agriculture, 2012. Engineering Classification of Earth Materials(Chapter 3). Part 631 Natl. Eng. Handb. 35.

(USDA) United States Department of Agriculture(NRCS), 1999. Soil Quality Test Kit Guide, Soil Quality Institute. doi:10.1037/t15144-000

Agisoft LLC, 2017. Agisoft PhotoScan Professional Edition User Manual.

Ali, F.H., Osman, N., 2008. Shear Strength of a Soil Containing Vegetation Roots. Soils Found. 48, 587–596. doi:10.3208/sandf.48.587

Allen, P., Jeffrey, A., Auguste, L., White, J., Dunbar, J., 2017. Application of a Simple Headcut Advance Model for Gullies. Earth Surf. Process. Landforms.

Allen, P.M., Arnold, J., Jakubowski, E., 1999. Prediction of Stream Channel Erosion Potential. Environ. Eng. Geosci. 3, 339–349. doi:10.2113/gseegeosci.V.3.339 Published on September 1999, First Published on September 01, 1999

Allen, P.M., Harmel, R.D., Arnold, J., Plant, B., Yelderman, J., King, K., 2005. Field data and flow system response in clay (vertisol) shale terrain, north-central Texas, USA. Hydrol. Process. 19, 2719–2736. doi:10.1002/hyp.5782

Allen, P.M., Maier, N., 1993. Impacts of Urbanization in the Blackland Prairie, in: Sharpless, R., Yelderman, J. (Eds.), The Texas Blackland Prairie: Land History, and Culture. Baylor University, Waco, p. 369.

Alonso, C. V., Bennett, S.J., Stein, O.R., 2002. Predicting head cut erosion and migration in concentrated flows typical of upland areas. Water Resour. Res. 38, 39-1-39–15. doi:10.1029/2001WR001173

Arnold, J.G., Potter, K.N., King, K.W., Allen, P.M., 2005a. Estimation of soil cracking and the effect on surface runoff in a Texas Blackland Prairie watershed. Hydrol. Process. 19, 589–603. doi:10.1002/hyp.5609

Arnold, J.G., Potter, K.N., King, K.W., Allen, P.M., 2005b. Estimation of soil cracking and the effect on surface runoff in a Texas Blackland Prairie watershed. Hydrol. Process. 19, 589–603. doi:10.1002/hyp.5609

Bartley, R., Hawdon, A., Post, D.A., Roth, C.H., 2007. A sediment budget for a grazed semi-arid catchment in the Burdekin basin, Australia. Geomorphology 87, 302–321. doi:10.1016/j.geomorph.2006.10.001

Bennett, S.J., Alonso, C. V, Prasad, S.N., Romkens, M.J.M., 2000. Experiments on headcut growth and migration in concentrated flows typical of upland areas. Water Resour. Res. 36, 1911–1922. doi:10.1029/2000WR900067

Bennett, S.J., Casalí, J., 2001. Effect of initial step height on headcut development in upland concentrated flows. Water Resour. Res. 37, 1475–1484. doi:10.1029/2000WR900373

Bland, W.L., Jones, C.A., 1993. Agricultural Technology Makes Its Mark, 1940 to the Present, in: Sharpless, R., Yelderman, J. (Eds.), The Texas Blackland Prairie: Land History, and Culture1. Baylor University, Waco, p. 369.

Boix-Fayos, C., Martínez-Mena, M., Arnau-Rosalén, E., Calvo-Cases, A., Castillo, V., Albaladejo, J., 2006. Measuring soil erosion by field plots: Understanding the sources of variation. Earth-Science Rev. 78, 267–285. doi:10.1016/j.earscirev.2006.05.005

Brakensiek, D.L., Osborn, H.B., 1979. Field Manual For Research in Agricultural Hydrology. Agric. Handb. doi:10.1016/0022-1694(65)90047-8

Brice, J.C., 1966. Erosion and Deposition in the Loess-Mantled Great Plains , Medicine Creek Drainage Basin , Nebraska Erosion and Deposition in the Loess-Mantled Great Plains , Medicine Creek Drainage Basin , Nebraska, Geological Survey Professional Paper 352 H.

Brodu, N., Lague, D., 2012. 3D terrestrial lidar data classification of complex natural scenes using a multi-scale dimensionality criterion: Applications in geomorphology. ISPRS J. Photogramm. Remote Sens. doi:10.1016/j.isprsjprs.2012.01.006

Bull, W.B., 1997. Discontinuous ephemeral streams. Geomorphology 19, 227–276. doi:10.1016/S0169-555X(97)00016-0

Castillo, C., Gómez, J.A., 2016. A century of gully erosion research: Urgency, complexity and study approaches. Earth-Science Rev. 160, 300–319. doi:10.1016/j.earscirev.2016.07.009

Castillo, C., Pérez, R., James, M.R., Quinton, J.N., Taguas, E. V., Gómez, J.A., 2012. Comparing the Accuracy of Several Field Methods for Measuring Gully Erosion. Soil Sci. Soc. Am. J. 76, 1319. doi:10.2136/sssaj2011.0390

Castro, J., Reckendorf, F., 1995. Effects of sediment on the aquatic environment : Potential NRCS actions to improve aquatic habitat.

Chintala, R.S., Allen, P., 1996. Stream Channel response in the Blackland Prairie. Baylor University.

Chu, S.T., 1978. Infiltration during an unsteady rain. Water Resour. Res. 14, 461–466. doi:10.1029/WR014i003p00461

Collins, O.B., Smeins, F.E., Riskind, D.H., 1975. Plant Communities of the Black-Land Prairie of Texas, in: Wali, M.K. (Ed.), Proceedings of the North American Prairie Conference, No. 4. University of North Dakota Press, Grand Forks, pp. 75–88.

Collison, A.J.C., 2001. The cycle of instability: stress release and fissure flow as controls on gully head retreat. Hydrol. Process. 15, 3–12. doi:10.1002/hyp.150

Couper, P., 2003. Effects of silt-clay content on the susceptibility of river banks to subaerial erosion. Geomorphology 56, 95–108. doi:10.1016/S0169-555X(03)00048-5

Cruse, R., Larson, W., 1977. Effect of soil shear strength on soil detachment due to raindrop impact. Soil Sci. Soc. Am. J. 41, 777–781. doi:10.2136/sssaj1977.03615995004100040034x

Daggupati, P., Sheshukov, A.Y., Douglas-Mankin, K.R., 2014. Evaluating ephemeral gullies with a process-based topographic index model. Catena 113, 177–186. doi:10.1016/j.catena.2013.10.005

DGM, AB, RM, 2017. Cloud Compare. GPL software.

Diamond, D.D., Smeins, F.E., 1993. The Native Plant Communities of the Blackland Prairie, in: Sharpless, R., Yelderman, J. (Eds.), The Texas Blackland Prairie: Land History, and Culture. Baylor University, Waco, p. 369.

Ding, L., Qin, F., Fang, H., Liu, H., Zhang, B., Shu, C., Deng, Q., Liu, G., Yang, Q., 2017. Morphology and controlling factors of the longitudinal profile of gullies in the Yuanmou dry-hot valley. J. Mt. Sci. 14, 674–693. doi:10.1007/s11629-016-4189-7

Dinka, T.M., Morgan, C.L.S., McInnes, K.J., Kishna, A.S., Daren Harmel, R., 2013. Shrink-swell behavior of soil across a Vertisol catena. J. Hydrol. 476, 352–359. doi:10.1016/j.jhydrol.2012.11.002

Dong, Y.., Xiong, D.., Su, Z.., Li, J.., Yang, D.., Zhai, J.., Lu, X.., Liu, .a, Shi, L.., 2013. Critical topographic threshold of gully erosion in the Yuanmou Dry-hot Valley in Southwestern China. Phys. Geogr. 34, 50–59. doi:10.1080/02723646.2013.778691

Dong, Y., Xiong, D., Su, Z., Li, J., Yang, D., Shi, L., Liu, G., 2014. The distribution of and factors influencing the vegetation in a gully in the Dry-hot Valley of southwest China. Catena 116, 60–67. doi:10.1016/j.catena.2013.12.009

Dudual, R., 1963. Dark Clay soils of Tropical and subtropical regions. Soil Sci. 95, 264–270.

Duncan, M.J., Wright, S.G., Brandon, T.L., 2014. Soil Strength and Slope Stability, 2nd ed. John Wiley & Sons Ltd, New Jersey.

El-Swaify, S.A., Dangler, E.W., Armstrong, C.L., 1982. Soil Erosion by Water in the Tropics. Res. Ext. Ser. 024 184. doi:10.1017/CBO9781107415324.004

Fan, C.C., Su, C.F., 2008. Role of roots in the shear strength of root-reinforced soils with high moisture content. Ecol. Eng. 33, 157–166. doi:10.1016/j.ecoleng.2008.02.013

Fitzjohn, C., Ternan, J.L., Williams, A.G., 1998. Soil moisture variability in a semi-arid gully catchment: Implications for runoff and erosion control. Catena 32, 55–70. doi:10.1016/S0341-8162(97)00045-3

Flores-Cervantes, J.H., Istanbulluoglu, E., Bras, R.L., 2006. Development of gullies on the landscape: A model of headcut retreat resulting from plunge pool erosion. J. Geophys. Res. Earth Surf. 111, 1–14. doi:10.1029/2004JF000226

Frankl, A., Poesen, J., Deckers, J., Haile, M., Nyssen, J., 2012. Gully head retreat rates in the semi-arid highlands of Northern Ethiopia. Geomorphology 173–174, 185–195. doi:10.1016/j.geomorph.2012.06.011

Frankl, A., Poesen, J., Scholiers, N., Jacob, M., Haile, M., Deckers, J., Nyssen, J., 2013. Factors controlling the morphology and volume (V)-length (L) relations of permanent gullies in the northern Ethiopian Highlands. Earth Surf. Process. Landforms 38, 1672–1684. doi:10.1002/esp.3405

Geissen, V., Kampichler, C., López-de Llergo-Juárez, J.J., Galindo-Acántara, A., 2007. Superficial and subterranean soil erosion in Tabasco, tropical Mexico: Development of a decision tree modeling approach. Geoderma 139, 277–287. doi:10.1016/j.geoderma.2007.01.002

Ghimire, S., Higaki, D., Bhattarai, T., 2013. Estimation of Soil Erosion Rates and Eroded Sediment in a Degraded Catchment of the Siwalik Hills, Nepal. Land 2, 370–391. doi:10.3390/land2030370

Gilley, J.E., Elliot, W.J., Laflen, J.M., Simanton, J.R., 1993. Critical shear stress and critical flow rates for initiation of rilling. J. Hydrol. 142, 251–271. doi:10.1016/0022-1694(93)90013-Y

Gómez-Gutiérrez, Á., Schnabel, S., Berenguer-Sempere, F., Lavado-Contador, F., Rubio-Delgado, J., 2014. Using 3D photo-reconstruction methods to estimate gully headcut erosion. Catena 120, 91–101. doi:10.1016/j.catena.2014.04.004

Grabowski, R.C., Droppo, I.G., Wharton, G., 2011. Erodibility of cohesive sediment: The importance of sediment properties. Earth-Science Rev. 105, 101–120. doi:10.1016/j.earscirev.2011.01.008

Graf, L., 1977. The rate law in fluvial geomorphology. Am. J. Sci. doi:10.2475/ajs.277.2.178

Greiner, J.H., 1982. Erosion and sedimentation by water in Texas: Texas Department of Water Resources Average Annual Rates Estimated in 1979.

Grissinger, E.H.R. of selected clay systems to erosion by water, 1966. Resistance of selected clay systems to erosion by water. Water Resour. Res. 2, 131–138. doi:10.1029/WR002i001p00131

Haigh, S.K., 2012. Mechanics of the Casagrande liquid limit test. Can. Geotech. J. 49, 1015. doi:http://dx.doi.org.ezproxy.baylor.edu/10.1139/T2012-066

Haigh, S.K., Vardanega, P.J., Bolton, M.D., 2013. The plastic limit of clays. Géotechnique 63, 435–440. doi:10.1680/geot.11.P.123

Hallmark, T.C., 1993. The Nature and Origin of the Blackland Soils, in: Sharpless, R.M., Yelderman, J.C. (Eds.), The Texas Blackland Prairie: Land History, and Culture. Baylor University, Waco, p. 369.

Hanson, G., Tejral, R.D., Hunt, S.L., Temple, D.M., 2010. Internal Erosion and Impact of Erosion Resistance, in: Proceedings of the 30th US Society on Dams Annual Meeting and Conferenc. pp. 773–784.

Hanson, G.J., Robinson, K.M., 1993. The Influence of Soil Moisture and Compaction On Spillway Erosion. Trans. ASAE 36, 1349–1352.

Hanson, G.J., Robinson, K.M., Cook, K.R., 2001. Prediction of Headcut Migration Using a Deterministic Approach. Trans. ASAE 44, 525–531.

Harmel, R.D., King, K.W., Richardson, C.W., Williams, J.R., 2003. Long-Term Precipitation Analyses For the Central Texas Blackland Prairie. Trans. ASAE 65, 1381–1388. doi:10.13031/2013.15449

Harmel, R.D., Richardson, C.W., King, K.W., Allen, P.M., 2006. Runoff and soil loss relationships for the Texas Blackland Prairies ecoregion. J. Hydrol. 331, 471–483. doi:10.1016/j.jhydrol.2006.05.033

Henderson, B., Wynn, T., Vaughan, D., 2006. Changes in Streambank Erodibility and Critical Shear. Virginia Polytechnic Institute and State University.

Hill, R.T., Walcott, C.D., 1901. Geography and geology of the Black and Grand prairies, Texas. Washington, Govt. Print. Off., US Geological Survey. Annual report, p. 666.

Hottenstein, J.D., Ponce-Campos, G.E., Moguel-Yanes, J., Moran, M.S., 2015. Impact of Varying Storm Intensity and Consecutive Dry Days on Grassland Soil Moisture. J. Hydrometeorol. 16, 106–117. doi:10.1175/JHM-D-14-0057.1

Hughes, A.O., Olley, J.M., Croke, J.C., McKergow, L.A., 2009. Sediment source changes over the last 250 years in a dry-tropical catchment, central Queensland, Australia. Geomorphology 104, 262–275. doi:10.1016/j.geomorph.2008.09.003

IUSS Working Group, 2015. World reference base for soil resources 2015 International soil classification system for naming soils and creating legends for soil maps, World Soil Resources Reports No. 106. FAO, Rome. doi:10.1017/S0014479706394902

James, L.A., Watson, D.G., Hansen, W.F., 2007. Using LiDAR data to map gullies and headwater streams under forest canopy: South Carolina, USA. Catena 71, 132–144. doi:10.1016/j.catena.2006.10.010

James, M.R., Robson, S., 2012. Straightforward reconstruction of 3D surfaces and topography with a camera: Accuracy and geoscience application. J. Geophys. Res. Earth Surf. 117, 1–17. doi:10.1029/2011JF002289

Kaiser, A., Neugirg, F., Rock, G., Müller, C., Haas, F., Ries, J., Schmidt, J., 2014. Small-scale surface reconstruction and volume calculation of soil erosion in complex Moroccan Gully morphology using structure from motion. Remote Sens. 6, 7050–7080. doi:10.3390/rs6087050

Kemper, W.D., Rosenau, R.C., 1984. Soil Cohesion as Affected by Time and Water Content. Soil Sci. Soc. Am. J. doi:10.2136/sssaj1984.03615995004800050009x

Kemper, W.D., Rosenau, R.C., Dexter, a. R., 1987. Cohesion Development in Disrupted Soils as Affected by Clay and Organic Matter Content and Temperature. Soil Sci. Soc. Am. J. 51, 860. doi:10.2136/sssaj1987.03615995005100040004x

Kishné, A.S., Ge, Y., Morgan, C.L.S., Miller (Retired), W.L., 2012. Surface Cracking of a Vertisol Related to the History of Available Water. Soil Sci. Soc. Am. J. 76, 548. doi:10.2136/sssaj2011.0060

Kishné, A.S., Morgan, C.L.S., Ge, Y., Miller, W.L., 2010. Antecedent soil moisture affecting surface cracking of a Vertisol in field conditions. Geoderma 157, 109–117. doi:10.1016/j.geoderma.2010.03.020

Klich, I., Wilding, L.P., Pfordresher, a. a., 1990. Close-Interval Spatial Variability of Udertic Paleustalfs in East Central Texas. Soil Sci. Soc. Am. J. doi:10.2136/sssaj1990.03615995005400020033x

Knapen, A., Poesen, J., Govers, G., Gyssels, G., Nachtergaele, J., 2007. Resistance of soils to concentrated flow erosion: A review. Earth-Science Rev. 80, 75–109. doi:10.1016/j.earscirev.2006.08.001

Lepore, B.J., Morgan, C.L.S., Norman, J.M., Molling, C.C., 2009. A Mesopore and Matrix infiltration model based on soil structure. Geoderma 152, 301–313. doi:10.1016/j.geoderma.2009.06.016

Li, G., Jackson, C.R., Kraseski, K.A., 2012. Modeled riparian stream shading: Agreement with field measurements and sensitivity to riparian conditions. J. Hydrol. 428–429, 142–151. doi:10.1016/j.jhydrol.2012.01.032

Line, D.E., Meyer, L.D., 1989. Evaluating interrill and rill erodibilities for soils of different textures. Trans. ASAE 32, 1995–1999.

Lowe, D.G., 2004. Distinctive image features from scale invariant keypoints. Int'l J. Comput. Vis. 60, 91–11020042. doi:http://dx.doi.org/10.1023/B:VISI.0000029664.99615.94

Maidment, D.R., 2002. Arc Hydro.

Marzolff, I., Poesen, J., 2009. The potential of 3D gully monitoring with GIS using high-resolution aerial photography and a digital photogrammetry system. Geomorphology 111, 48–60. doi:10.1016/j.geomorph.2008.05.047

McFarland, G., 1993. The Geology of the Blackland Prairie, in: Sharpless, R.M., Yelderman, J.C. (Eds.), The Texas Blackland Prairie: Land, History, and Culture. Baylor University, Waco, p. 369.

McNamara, J.P., Ziegler, A.D., Wood, S.H., Vogler, J.B., 2006. Channel head locations with respect to geomorphologic thresholds derived from a digital elevation model: A case study in northern Thailand. For. Ecol. Manage. 224, 147–156. doi:10.1016/j.foreco.2005.12.014

Mein, R.G., Larson, C.L., 1973. Modeling infiltration during a steady rain. Water Resour. Res. 9, 384–394. doi:10.1029/WR009i002p00384

Meyer, L.D., Foster, G.R., Nikolov, S., 1975. Effect of Flow Rate and Canopy on Rill Erosion. Trans. ASAE 18, 0905–0911. doi:10.13031/2013.36705

Miller, W.L., Kishné, A.S., Morgan, C.L.S., 2010. Vertisol Morphology, Classification, and Seasonal Cracking Patterns in the Texas Gulf Coast Prairie. Soil Surv. Horizons 51, 10–16.

Mitchell, J.K., 1964. Shearing Resistance Of Soils As A Rate Process. J. Soil Mech. Found. Div. Am. Soc. Civ. Eng. 90, 29–62.

Montgomery, J.A., 1993. The Nature and Origin of the Blackland Prairies of Texas, in: Sharpless, R., Yelderman, J. (Eds.), The Texas Blackland Prairie: Land History, and Culture. Baylor University, Waco, p. 369.

Nazari Samani, A., Ahmadi, H., Mohammadi, A., Ghoddousi, J., Salajegheh, A., Boggs, G., Pishyar, R., 2009. Factors Controlling Gully Advancement and Models Evaluation (Hableh Rood Basin, Iran). Water Resour. Manag. 24, 1531–1549. doi:10.1007/s11269-009-9512-4

Nyssen, J., Poesen, J., Veyret-Picot, M., Moeyersons, J., Haile, M., Deckers, J., Dewit, J., Naudts, J., Teka, K., Govers, G., 2006. Assessment of gully erosion rates through interviews and measurements: A case study from northern Ethiopia. Earth Surf. Process. Landforms 31, 167–185. doi:10.1002/esp.1317

Occupational Safety and Health Administration[OSHA], 2017. Regulations(Standards-29 CFR 1926 Sub-part P App A - Soil Classification) [WWW Document]. URL https://www.osha.gov/pls/oshaweb/owadisp.show_document?p_table=STANDARDS&p_id=10931 (accessed 5.24.17).

Ollobarren, P., Capra, A., Gelsomino, A., La Spada, C., 2016. Effects of ephemeral gully erosion on soil degradation in a cultivated area in Sicily (Italy). Catena 145, 334–345. doi:10.1016/j.catena.2016.06.031

Osborn, H.B., Simanton, J.R., 1986. Gully migration on a southwest rangeland watershed. J. Range Manag. 39, 558–561. doi:10.2307/3898771

Osman, N., Barakbah, S.S., 2006. Parameters to predict slope stability-Soil water and root profiles. Ecol. Eng. 28, 90–95. doi:10.1016/j.ecoleng.2006.04.004

Ozment, R., 1993. Farming in the Blacklands During the Great Depression, in: Sharpless, R., Yelderman, J. (Eds.), The Texas Blackland Prairie: Land History, and Culture. Baylor University, Waco, p. 369.

Pathak, P., Sudi, R., Wani, S.P., Sahrawat, K.L., 2013. Hydrological behavior of Alfisols and Vertisols in the semi-arid zone: Implications for soil and water management. Agric. Water Manag. 118, 12–21. doi:10.1016/j.agwat.2012.11.012

Pathak, P., Wani, S.P., Sudi, R., 2005. Gully Control in SAT Watersheds, International Crops Research Institute for the Semi-arid Tropics. Patancheru.

Patton, P.C., Schümm, S. a, 1975. Gully Erosion, Northwestern Colorado: A Threshold Phenomenon. Geology 3, 88–90.

Perroy, R.L., Bookhagen, B., Asner, G.P., Chadwick, O.A., 2010. Comparison of gully erosion estimates using airborne and ground-based LiDAR on Santa Cruz Island, California. Geomorphology 118, 288–300. doi:10.1016/j.geomorph.2010.01.009

Ploumis-Devick, E., 1985. Plunge Pool Erosion In Cohesive Channels below a free overfall. Soc. Change. The Ohio State University.

Poesen, J., Nachtergaele, J., Verstraeten, G., Valentin, C., 2003. Gully erosion and environmental change: Importance and research needs. Catena 50, 91–133. doi:10.1016/S0341-8162(02)00143-1

Poesen, J., Verstraeten, G., Wijdenes, D.J.O., Wesemael, B. van, 2002. Gully Erosion in Dryland Environments . Dryland Rivers:Hydrology and Geomorphology of Semi-arid Channels. John Wiley & Sons Ltd, Chichester.

Poesen, J.W., Vandaele, K., Wesemael, B.V. a. N., 1996. Contribution of gully erosion to sediment production on cultivated lands and rangelands, in: Erosion and Sediment Yield: Global and Regional Perspectives (Proceedings of the Exeter Symposium). International Association of Hydrological Sciences, pp. 251–266.

Poff, N.L., Allan, J.D., Bain, M.B., Karr, J.R., Prestegaard, K.L., Richter, B.D., Sparks, R.E., Stromberg, J.C., 1997. A paradigm for river conservation and restoration. Bioscience 47, 769–784. doi:10.2307/1313099

PRISM Climate Group, 2017. Oregon State University [WWW Document]. URL http://www.prism.oregonstate.edu/explorer/ (accessed 5.6.17).

Prosdocimi, M., Calligaro, S., Sofia, G., Dalla Fontana, G., Tarolli, P., 2015. Bank erosion in agricultural drainage networks: New challenges from structure-from-motion photogrammetry for post-event analysis. Earth Surf. Process. Landforms 40, 1891–1906. doi:10.1002/esp.3767

Puppala, A.J., Manosuthikij, T., Chittoori, B.C.S., 2013. Swell and shrinkage characterizations of unsaturated expansive clays from Texas. Eng. Geol. 164, 187–194. doi:10.1016/j.enggeo.2013.07.001

Radoane, M., Ichim, I., Radoane, N., 1995. Gully distribution and development in Moldavia, Romania. Catena 24, 127–146. doi:10.1016/0341-8162(95)00023-L

Rawls, W.J., Brakensiek, D.L., Miller, N., 1983. Green-ampt Infiltration Parameters from Soils Data. J. Hydraul. Eng. 109, 62–70. doi:10.1061/(ASCE)0733-9429(1983)109:1(62)

Rengers, F.K., Tucker, G.E., 2015. The evolution of gully headcut morphology: a case study using terrestrial laser scanning and hydrological monitoring. Earth Surf. Process. Landforms 40, 1304–1317. doi:10.1002/esp.3721

Richardson, C.W., 1993. Disappearing Land:Erosion in the Blacklands, in: Sharpless, R., Yelderman, J. (Eds.), The Texas Blackland Prairie: Land History, and Culture. Baylor University, Waco, p. 369.

Rieke-Zapp, D.H., Nichols, M.H., 2011. Headcut retreat in a semiarid watershed in the southwestern United States since 1935. Catena 87, 1–10. doi:10.1016/j.catena.2011.04.002

Riskind, D.H., Collins, O.B., 1975. The Black-Land Prairie of Texas Conservation of Representative Climax Remnants, in: Wali, M.K. (Ed.), Proceedings of the North American Prairie Conference, No. 4. University of North Dakota Press, Grand Forks, pp. 361–368.

Robinson, K.M., 1996. Gully Erosion And HeadCut Advance. Oklahoma State University. doi:10.16953/deusbed.74839

Robinson, K.M., Hanson, G.J., 1996. Influence of Backwater on gully headcut advance, in: Transactions of the ASAE. North American Water and Environment Congress & Destructive Water, pp. 33–38.

Robinson, K.M., Hanson, G.J., 1995a. Gully headcut advance. Trans. Am. Soc. Agric. Eng. 39, 33–38.

Robinson, K.M., Hanson, G.J., 1995b. Large-Scale HEadCut Erosion Testing. Trans. ASAE 38, 429–434.

Rosone, M., Airò Farulla, C., Ferrari, A., 2016. Shear strength of a compacted scaly clay in variable saturation conditions. Acta Geotech. 11, 37–50. doi:10.1007/s11440-015-0379-7

Saxton, K., Rawls, W., 2006. Soil Water Characteristic Estimates by Texture and Organic Matter for Hydrologic Solutions. Soil Sci. Soc. Am. J. 70, 1569–1578. doi:10.2136/sssaj2005.0117

Saxton, N.E., Olley, J.M., Smith, S., Ward, D.P., Rose, C.W., 2012. Gully erosion in sub-tropical south-east Queensland, Australia. Geomorphology 173–174, 80–87. doi:10.1016/j.geomorph.2012.05.030

Shan, H., Shen, J., Kilgore, R., Kerenyi, K., 2015. Scour in Cohesive Soils.

Sheridan, G.J., So, H.B., Loch, R.J., Walker, C.M., 2000. Estimation of erosion model erodibility parameters from media properties. Aust. J. Soil Res. doi:10.1071/SR99041

Simon, A., Rinaldi, M., 2013. Incised Channels: Disturbance, Evolution and the Roles of Excess Transport Capacity and Boundary Materials in Controlling Channel Response. Treatise Geomorphol. doi:10.1016/B978-0-12-374739-6.00255-4

Skempton, A.W., 1953. The Colloidal “Activity” of Clays, in: 3rd International Conference of Soil Mechanics and Foundation Engineering. Switzerland, p. 57.

Smith, J.T., Welborn, C.T., 1967. Hydrologic Studies Of Small Watersheds: Pin Oak Creek, Trinity River Basin, Texas, Texas Water Development Board. Austin, Texas.

Snavely, N., Seitz, S.M., Szeliski, R., 2006. Photo tourism: Exploring Photo Collections in 3D. ACM Trans. Graph. 25, 835–846. doi:10.1145/1141911.1141964

Stein, O.R., LaTray, D. a., 2002. Experiments and modeling of head cut migration in stratified soils. Water Resour. Res. 38, 20-1-20–12. doi:10.1029/2001WR001166

Stocking, M.A., 1980. Examination of the factors controlling gully growth, in: Boodt, D., Gabriels, M. (Eds.), Assessment of Erosion. John Wiley & Sons, Chichester, pp. 505–520.

Swanson, M.L., Kondolf, G.M., Boison, P.J., 1989. An example of rapid gully initiation and extension by subsurface erosion: Coastal San Mateo County, California. Geomorphology 2, 393–403. doi:10.1016/0169-555X(89)90023-8

Tebebu, T.Y., Abiy, A.Z., Zegeye, A.D., Alemie, T.C., 2010. Assessment of Hydrological Controls on Gully Formation and UPLAND EROSION NEAR LAKE TANA, NORTHERN HIGHLANDS OF ETHIOPIA, in: October. 2nd Joint Federal Interagency Conference, Las Vegas.

Telles, T.S., Guimarães, M. de F., Dechen, S.C.F., 2011. The Costs of Soil Erosion 35, 287–298.

Thomas, J.T., Iverson, N.R., Burkart, M.R., Kramer, L.A., 2004. Long-term growth of a valley-bottom gully, Western Iowa. Earth Surf. Process. Landforms 29, 995–1009. doi:10.1002/esp.1084

Thompson, C.M., 1993. More from Less:Greater Demand from Fewer Acres of Productive Soils, in: Sharpless, R., Yelderman, J. (Eds.), The Texas Blackland Prairie: Land History, and Culture. Baylor University, Waco, p. 369.

Tonkin, T.N., Midgley, N.G., Graham, D.J., Labadz, J.C., 2014. The potential of small unmanned aircraft systems and structure-from-motion for topographic surveys: A test of emerging integrated approaches at Cwm Idwal, North Wales. Geomorphology 226, 35–43. doi:10.1016/j.geomorph.2014.07.021

Trimble Navigation, 2003. Real-Time Kinematic (RTK) Systems, D. ed, Real-Time Kinematic Surveying Training Guide. Trimble Navigation Limited, California.

Ullman, S., 1979. The Interpretation of Structure from Motion. Proc. R. Soc. London. Ser. B, Biol. Sci. 203, 405–426.

University of Texas, 1979. Geologic Atlas of Texas: Waco Sheet.

US Army Corps of Engineers, 2003. Engineering and Design Slope Stability. USACE Publ. Em-1110-2-, 205. doi:10.1016/0148-9062(75)90139-4

USDA-NRCS, 2009. National Engineering Handbook Chapter 7: Hydrologic Soil Groups, Part 630 Hydrology National Engineering Handbook. doi:https://directives.sc.egov.usda.gov/OpenNonWebContent.aspx?content=17757.wba

Valentin, C., Poesen, J., Li, Y., 2005. Gully erosion: Impacts, factors and control. Catena 63, 132–153. doi:10.1016/j.catena.2005.06.001

Van Den Elsen, E., Xie, Y., Liu, B., Stolte, J., Wu, Y., Trouwborst, K., Ritsema, C.J., 2003. Intensive water content and discharge measurement system in a hillslope gully in China. Catena 54, 93–115. doi:10.1016/S0341-8162(03)00059-6

Vandekerckhove, L., Poesen, J., Govers, G., 2003. Medium-term gully headcut retreat rates in Southeast Spain determined from aerial photographs and ground measurements. Catena 50, 329–352. doi:10.1016/S0341-8162(02)00132-7

Vanmaercke, M., Poesen, J., Van Mele, B., Demuzere, M., Bruynseels, A., Golosov, V., Bezerra, J.F.R., Bolysov, S., Dvinskih, A., Frankl, A., Fuseina, Y., Guerra, A.J.T., Haregeweyn, N., Ionita, I., Makanzu Imwangana, F., Moeyersons, J., Moshe, I., Nazari Samani, A., Niacsu, L., Nyssen, J., Otsuki, Y., Radoane, M., Rysin, I., Ryzhov, Y. V., Yermolaev, O., 2016. How fast do gully headcuts retreat? Earth-Science Rev. 154, 336–355. doi:10.1016/j.earscirev.2016.01.009

Vanwalleghem, T., Poesen, J., Nachtergaele, J., Verstraeten, G., 2005. Characteristics, controlling factors and importance of deep gullies under cropland on loess-derived soils. Geomorphology 69, 76–91. doi:10.1016/j.geomorph.2004.12.003

Vardanega, P.J., Haigh, S.K., 2014. The undrained strength – liquidity index relationship. Can. Geotech. J. 5, 1073–1086. doi:10.1139/cgj-2013-0169

Verstraeten, G., Poesen, J., de Vente, J., Koninckx, X., 2003. Sediment yield variability in Spain: A quantitative and semi-qualitative analysis using reservoir sedimentation rates. Geomorphology 50, 327–348. doi:10.1016/S0169-555X(02)00220-9

Wang, R., Zhang, S., Pu, L., Yang, J., Yang, C., Chen, J., Guan, C., Wang, Q., Chen, D., Fu, B., Sang, X., 2016. Gully Erosion Mapping and Monitoring at Multiple Scales Based on Multi-Source Remote Sensing Data of the Sancha River Catchment, Northeast China. ISPRS Int. J. Geo-Information 5, 200. doi:10.3390/ijgi5110200

Westoby, M.J., Brasington, J., Glasser, N.F., Hambrey, M.J., Reynolds, J.M., 2012. "Structure-from-Motion" photogrammetry: A low-cost, effective tool for geoscience applications. Geomorphology 179, 300–314. doi:10.1016/j.geomorph.2012.08.021

Whitford, J.A., Newham, L.T.H., Vigiak, O., Melland, A.R., Roberts, A.M., 2010. Rapid assessment of gully sidewall erosion rates in data-poor catchments: A case study in Australia. Geomorphology 118, 330–338. doi:10.1016/j.geomorph.2010.01.013

Widodo, S., Ibrahim, A., Hong, S., 2012. Analysis of different equations of undrained shear strength estimations using Atterberg Limits on Pontianak Soft Clay. Challenges Mod. Technol. 3, 46–50.

Wilding, L.., Williams, D., Miller, W., Cook, T., Eswaran, H., 1991. Close interval spatial variability of Vertisols: a case study in Texas. Proc. Int. Soil Correl. Meet.

Wolman, M.G., 1959. Factors Influencing Erosion of a Cohesive River Bank. Am. J. Sci. doi:10.2475/ajs.257.3.204

Wu, Y., Cheng, H., 2005. Monitoring of gully erosion on the Loess Plateau of China using a global positioning system. Catena 63, 154–166. doi:10.1016/j.catena.2005.06.002

Xu, M., Li, Q., Wilson, G., 2016. Degradation of soil physicochemical quality by ephemeral gully erosion on sloping cropland of the hilly Loess Plateau, China. Soil Tillage Res. 155, 9–18. doi:10.1016/j.still.2015.07.012

Yelderman, F., 1993. Disappearing Water:Increasing Needs from a Diminishing Supply, in: Sharpless, R., Yelderm (Eds.), The Texas Blackland Prairie: Land History, and Culture. Baylor University, Waco, p. 369.

Yelderman, J.C.J., 1993. The Water: Nature and Distribution in the Blacklands, in: Sharpless, R., Yelderman, J. (Eds.), The Texas Blackland Prairie: Land History, and Culture. Baylor University, Waco, p. 369.

Zegeye, A.D., Langendoen, E.J., Stoof, C.R., Tilahun, S.A., Dagnew, D.C., Zimale, F.A., Guzman, C.D., Yitaferu, B., Steenhuis, T.S., 2016. Morphological dynamics of gully systems in the subhumid Ethiopian Highlands: the Debre Mawi watershed. Soil 2, 443–458. doi:10.5194/soil-2-443-2016

Zgłobicki, W., Baran-Zgłobicka, B., Gawrysiak, L., Telecka, M., 2014. The impact of permanent gullies on present-day land use and agriculture in loess areas (E. Poland). Catena 126, 28–36. doi:10.1016/j.catena.2014.10.022